

## **Nanocluster fractal electrical conductivity in thin films on a solid surface: dimensional models of different configurations and demonstration of results in a laser experiment**

© Dmitry N. Bukharov<sup>a</sup>, Alexey O. Kucherik<sup>a</sup>, Sergei M. Arakelian<sup>a</sup>✉

<sup>a</sup> Vladimir State University named after Alexander and Nikolay Stoletovs,  
87, Gorky St., Vladimir, 600000, Russian Federation

✉ arak@vlsu.ru

**Abstract:** Models for the formation of nanocluster fractal structures of various configurations are considered within the framework of a number of approaches in the aspect of controlling their electrophysical characteristics, and the results of some experiments in this direction by laser experiment are presented. Emphasis is placed on the discussion and analysis of the following issues: physical principles and models for the electrical conductivity in topological nanostructures; local fields in nanoscale and their contribution to the gain coefficient for electrical conductivity in aspect of parameters of the medium and the geometry factors for roughness; experimental technique; current-voltage characteristics and mechanisms of electrical conduction for topological nanostructures under different conditions. At the same time, occurrence of conduction electropaths, and also the algorithms and models considered for calculating of electrical conductivity for nanostructures of different configuration are analyzed, experimental results and their interpretation are presented, and the role of photoconductivity were studied in such nanostructures. The results obtained can be useful in the development of certain elements and systems of nanotopological electrophysics and nanophotonics based on new physical principles.

**Keywords:** nanoclusters; fractal configurations; topological electrical conductivity; dimensional effects; modeling and experiments with different mechanisms of electrical conductivity in various conditions.

**For citation:** Bukharov DN, Kucherik AO, Arakelian SM. Nanocluster fractal electrical conductivity in thin films on a solid surface: dimensional models of different configurations and demonstration of results in a laser experiment. *Journal of Advanced Materials and Technologies*. 2023;8(3):227-251. DOI: 10.17277/jamt.2023.03.pp.227-251

## **Нанокластерная фрактальная электропроводимость в тонких пленках на твердой поверхности: размерные модели разных конфигураций и демонстрация результатов в лазерном эксперименте**

© Д. Н. Бухаров<sup>a</sup>, А. О. Кучерик<sup>a</sup>, С. М. Аракелян<sup>a</sup>✉

<sup>a</sup> Владимирский государственный университет  
им. Александра Григорьевича и Николая Григорьевича Столетовых,  
ул. Горького, 87, Владимир, 600000, Российская Федерация

✉ arak@vlsu.ru

**Аннотация:** Рассмотрены модели формирования нанокластерных фрактальных структур разной конфигурации в рамках ряда подходов в аспекте управления их электрофизическими характеристиками и приведены результаты некоторых экспериментов по данному направлению в лазерных схемах. Акценты сделаны на обсуждении и анализе следующих вопросов: физические принципы и модели для электропроводимости топологических наноструктур; локальные поля на наномасштабах и их роль в зависимости от параметров среды и геометрии шероховатости в коэффициентах усиления для электропроводимости; методика эксперимента; вольт-амперные характеристики топологических наноструктур и механизмы электропроводности в разных условиях эксперимента. При этом исследованы возникающие дорожки электропроводимости, рассмотрены алгоритмы и модели для расчета электропроводимости, проанализированы наноструктуры разной конфигурации, приведены

демонстрационные экспериментальные результаты и дана их интерпретация, оценена роль фотопроводимости в подобных наноструктурах. Полученные результаты могут быть полезны при разработке различных элементов и систем топологической наноэлектрофизики и нанофотоники на новых физических принципах.

**Ключевые слова:** нанокластеры; фрактальные конфигурации; топологическая электропроводимость; размерные эффекты; модели и эксперименты с разными механизмами электропроводимости в определенных условиях.

**Для цитирования:** Bukharov DN, Kucherik AO, Arakelian SM. Nanocluster fractal electrical conductivity in thin films on a solid surface: dimensional models of different configurations and demonstration of results in a laser experiment. *Journal of Advanced Materials and Technologies. 2023;8(3):227-251. DOI: 10.17277/jamt.2023.03.pp.227-251*

## 1. Introduction

Electrophysics of thin-film systems with nanoclusters (nanodots) with different controlled topology on the surface of a solid body, obtained in a laser experiment, has a number of fundamental features [1]. Such nanostructured surface configurations, related in terms of electrophysics for inhomogeneous media to granular/island objects [2], are controlled by different methods of laser deposition of almost any substance and/or alloy with different concentrations of defects in nanocomposites onto a solid surface, in particular, using the process of laser ablation of a material in a liquid [1, 3]. Thus, the possibility of synthesizing structures with arbitrary elemental/chemical compositions appears.

The fundamental physical fact here is that this process occurs under normal external conditions, but nevertheless, extreme conditions are realized in local areas even when exposed to relatively low-power laser radiation. This leads to a number of effects; secondly, a special allotropic form of carbon, carbene [1, 4, 5] with 1D carbon chains, is realized. The production of such long 1D chains – Long Liner Carbon Chain (LLCC) – has now become a routine process in a certain procedure of laser ablation of carbon materials in association with noble metals [6–10].

When considering the possibility of a cardinal change in a given way in the electrical characteristics of such systems, determined by an increase in electrical conductivity due to surface conductivity with cluster boundaries, topological nanocluster structures of the fractal type are of greater interest, both in fundamental and applied aspects, since the electrical conductivity can vary by many orders of magnitude [7, 10, 11]. In this case, the electrical conductivity is defined here as the specific conductivity, depending on the dimension  $D$  of the object (from 1 to 3), in units of  $\sigma_D$  [ $\text{Ohm}^{-1}\text{cm}^{2-D}$ ]. The control parameter is the characteristics of the topological structures, the change of which plays a role similar to the change in temperature during ordinary phase transitions with a certain order parameter.

In this aspect, the search for new materials with the required functional characteristics is similar to inducing the corresponding topological configurations on a solid surface in a laser experiment.

In similar size-quantized semiconductor-type systems, the distance between the  $\delta\varepsilon$  energy levels in a cluster is determined by the density of states at the Fermi level in a  $g_F$  bulk sample and the average volume of one  $a^3$  cluster according to the relation [12]:  $\delta\varepsilon = (g_F a^3)^{-1}$ , where  $\delta\varepsilon \approx 10\text{K} \sim 10^{-3}\text{ eV}$  at  $a = 5\text{ nm}$ .

In this regard, there is a simple physical analogy with such a key problem as the achievement of high-temperature superconductivity ( $\sim 300\text{ K}$ , which is  $\approx 0.03\text{ eV}$  in energy units), for which, in the general case, the necessary condition for this, in fact, directed delocalization is, firstly, a decrease in the scattering of charge carriers – electrons on phonons, and secondly, a certain small energy band gap near the Fermi level (in the presence of a sharp Fermi surface), leading to electron pairing (Cooper pairs) with a virtual exchange of phonons with energy, exceeding the energy of thermal fluctuations [13]. An important feature of precisely neutral nanoclusters is their charge neutrality; therefore, the mechanism of such pairing has the nature of van der Waals attraction.

In this case, the band gap itself (the lower boundary of the conduction band) also depends on the number of nanolayers on the substrate, and it will decrease with their growth, tending to a normal metal in the limit.

Although the detailed nature of high-temperature superconductivity is not yet completely clear [14], the definition of the relevant physical principles for identifying trends and regularities for increasing electrical conductivity in topological nanocluster structures with a selectable inhomogeneous configuration on the dielectric surface of a solid (systems with “voids” – cf. [10, 11, 15]), can be considered as an analogy with the electrophysics of topological insulators [2, 16, 17].

The physics of such processes is determined by electron interference (the Aronov–Altshuler effect

[13, 18, 19]), which can also be preserved at room temperature. This leads to a quantum correction in units of the conductance quantum (conductance  $\sim e^2/h$ , where  $e$  is the charge of an electron with the reciprocal dimension to the resistance  $\sim (1/4110 \text{ Ohm})$ . The electrical conductivity itself depends on the dimension of the system, but when this correction becomes positive, then a superconducting state can arise [12, 13].

The presence of “voids” in the topological nanostructure can be considered in terms of the analogy of the insulator-metal/superconductor transition [17]. In this case, the role of quantum tunneling effects between delocalized states both between clusters and within one cluster increases in surface nanoclusters. They can be weakened by the Coulomb blockade effect, but this does not occur for a 5 nm cluster at high temperatures  $\sim 300 \text{ K}$  under conditions when the surface electrical conductivity increases inversely with the thickness of the surface layer (the nanoobject is located on a solid surface like a film) [2].

Thus, such a set of nanoclusters on a solid surface can lead to a significant increase in the electrical conductivity characteristics, but in contrast to the hopping conductivity of charge carriers between localized states, tunneling is about their transition between delocalized states [2, 13, 18, 19]. This is determined, on the one hand, by the size of an isolated conducting cluster and the density of states at the Fermi level in it, and, on the other hand, by the interaction between the clusters themselves [2, 12]. It is this latter factor that distinguishes such a nanocluster structure from a bulky bulk sample in terms of the value of the critical temperature of superconductivity, which depends on the particular topology and energy barriers that arise.

For the electrical resistance of fractal structures, of greatest interest are fractal objects, which with a controlled configuration [1] can be obtained, for example, by laser deposition of nanoparticles from colloidal systems onto a solid substrate [10, 20]. Such systems can easily arise in a controlled and universal procedure for laser ablation of various materials in liquids [3]. In this case, depending on the topological structure, for example, for a semiconductor nanocluster system, here it becomes possible to control the band gap with its modified boundaries to implement direct and indirect electron transitions from the valence band to the conduction band [2, 19]. In the second case of indirect transitions, the process proceeds with the participation/exchange of phonons. This makes it possible to realize paired states of electrons under certain conditions.

On the other hand, the very presence of “voids” (pores) with a certain distribution function can serve as an analogue of doping in the presence of such vacancies. Similar effects in a polydisperse medium are characteristic of a non-ideal surface and are considered with different roughness models. They affect the value of the work of the electron quantum yield and its depth for such nanostructured heterogeneous media with the manifestation of size effects [10, 18].

It is important to emphasize that, in such fractal-type nanocluster structures, the attainment of the superconducting state does not necessarily lead to a drop in the electrical resistance to zero along the entire length of the sample [2, 12]. This is due to the effect of tunneling through “voids” between clusters, if the main resistance in the current channels is determined precisely by the transition of charge carriers through these “voids”. In a sense, here we can talk about analogies with the Josephson effect in superconductivity through a contact, when the application of an external constant electric field of voltage  $U$  to such a tunnel contact already passes with the presence of dissipation [2, 13, 18, 19]. In this case, the voltage drop  $\Delta U = RI + U$  (where  $R$  is the resistance,  $I$  is the current flowing in the circuit) has the usual form for alloys. The peculiarity of a tunnel junction with a superconductor (in the presence of  $R$  in the circuit) is associated with the value of  $I$  determined by the phase difference on both sides of the contact  $\phi_{12}$ :  $I \sim \sin \phi_{12}$ .

In such cluster-fractal structures, one can draw an analogy with the usual current propagation, for example, along a wire with a large length and a small cross section, when the current trajectories look like winding lines in the gaps between clusters in the form of Brownian motion in the fractal structure [2, 21].

On the other hand, they can lead to complex helicoidal structures, in particular, in graphene layers, and twisted configurations, which significantly affect their electrophysical characteristics [22]. Moreover, such twisting can effectively lead to states similar to the states of electrons with opposite spins, forming Cooper pairs (correlations in the momentum space with a probability of zero momentum sum and with symmetry with respect to time reversal) [12, 13]. But everything here is determined by the specific configuration of the resulting topological nanostructure.

Of fundamental importance is the fact that, by changing its configuration in a controlled way even at the stage of its creation, one can, in particular, radically change the electronic states of the sample substance and the shape of its Fermi surface, and

therefore influence the electrical resistance of the resulting sample [8, 10, 11].

Another feature of such topological fractal structures in the aspect of considering the tendency to the superconducting state is that we are talking here about granular inhomogeneous objects, where a second-order phase transition to the state of weak superconductors can be realized. For them, it is a mandatory criterion to study the influence and role of an external magnetic field and the depth of its penetration into the medium when a superconducting state appears, but in this topological case this requirement does not play a special role [13, 18, 19]. Moreover, the process of formation of such structures can occur under conditions of negative surface tension in the dynamics of the formed nanoclusters (conditions of a local isobaric state – cf. [23]), but with the fixation of usually unstable similar objects and their further existence under normal conditions. This is typical, as mentioned above, for the process of laser ablation of a graphite target in a liquid, for example, during the formation of micronanodiamonds. Therefore, the requirement of minimum energy for the final stable state of the system is fulfilled [14, 18].

However, for such nanostructured objects and their compositions, there is a real physical problem when using the numerical values of the material macroscopic parameters of a massive medium for such micro-nanoscale systems. But in the case of clarification of the ongoing trends, such an approximation is apparently still possible and / or it is necessary to renormalize the parameters used, for example, the value of resistivity  $\rho$  should be considered as a certain calibration coefficient. In particular, in [10, 11], jumps in electrical resistance by a factor of  $10^4$  were observed in the experiment for a certain topology of fractal objects in thin surface layers on solid samples. They are probably not reduced to obvious short-circuit currents, since, firstly, they are smoothly and reversibly regulated depending on the topology and its dimensions in accordance with the model estimates, and secondly, in the experiment they demonstrate a clear dependence on a specific value topological dimension.

Obviously, for the problem of real and possible achievement with a trend towards the required superconducting state, it is necessary to use correct measured material parameters for samples with the selected appropriate elemental composition and realized topology.

The fractal structures under consideration were modeled by us within the framework of different approaches, taking into account the achievements of

laser methods, and the results obtained are presented in the corresponding sections of this article.

Section 1 considers the physical principles and models for the electrical conductivity of topological structures. Section 2 discusses local fields and gains for electrical conductivity under different conditions. Section 3 deals with the experimental technique. Section 4 presents the current-voltage characteristics (CVCs) and discusses the mechanisms of electrical conductivity, as well as demonstration experimental results and their interpretation; in addition, issues with the representation of the role of photoconductivity are considered and calculations are performed for the temperature field.

In the Conclusion, the main conclusions on the work are presented in the aspect of their consideration for topical problems of modern topological nanoelectrophysics and nanophotonics for thin-film systems.

## **2. Materials and methods: physical principles and models for the electrical conductivity of topological structures**

When forming a nanocluster of electrical conductivity, i.e., a platform within which the current is most likely to flow [2, 24, 25], it is necessary to select an electrical conductivity track in it, along which the electric current can flow, taking into account the topological structure of the simulated film. This makes it possible to estimate the current-voltage characteristics of such a fractal structure based on the standard Ohm's law.

In this case, 2 types of configurations of the synthesized topology are possible, firstly, a network of closely spaced nanoclusters/islands connected to each other by conducting "bridges", and, secondly, a system of nanoclusters/islands isolated by large distances from each other, which can be characterized by a dielectric type of conductivity [2, 18, 26–29].

In the first case, we are talking about a continuous path of current flow. Therefore, such a 2D area can be classified as a nanofilm with a percolation type of electrical conductivity. In the second case, there are no continuous paths of current flow, and the mechanism of electrical conductivity, when it occurs, should have a jump-like character.

According to the physical picture, one of the factors affecting the current-voltage characteristics of nanostructures with object sizes of  $\sim 10\text{--}100$  nm is the total electrical resistance  $R$  of a microcontact formed in an inhomogeneous structure with a characteristic



length of the resistor section determined by the mean free path of an electron [2, 21]:

$$R = \frac{16\rho^\infty\lambda^\infty}{\pi d^2} \left( 1 + \frac{L}{d} + \frac{d}{\lambda^\infty} \right), \quad (1)$$

where  $d$  is contact diameter,  $\lambda$  is the mean free path of electrons in a bulk material,  $\rho$  is the electrical resistivity of the contacting particles of the material,  $L$  is the length of the microcontact.

Then the electric current in this system of contacting nanoparticles will flow only through the contact surfaces - areas with an area tending to zero.

We mean the formation of a plurality of longitudinal channels for the flow of current, which significantly complicates the transverse propagation of the current (there is no integral/homogeneous cross section for a section of the conductor circuit). In this case, to estimate the total electrical resistance of the microcontact, it is necessary to modify the expression for the standard Ohm's law for the circuit section, from which relation (1) is also derived.

In such nanocluster fractal structures with a given topology in thin-film flat solid-state samples, the calculation of the electrical resistance  $R$  of a circuit section (current path) with a fractal relief (here we are talking about static structural inhomogeneities, in contrast to dynamic – temperature ones) can be performed according to the following model relation [21]:

$$R = A\rho \frac{l_n(L_0/l_n)^D}{S_n(S_0/S_n)^{2-D_1}}, \quad (2)$$

where  $\rho$  is the resistivity of the bulk material,  $A$  is a normalization coefficient that takes into account the scale of the inhomogeneity,  $L_0$  is the length of the observed curve along the line from the initial to the final points of the microcontacts when measuring the current on the conducting surface,  $l_n$  is the length of the set of coatings (the distance between neighboring clusters),  $S_n$  is the area of the minimum coverage element,  $S_0$  is the area of the ellipse into which the averaged relief of the transverse cut is inscribed,  $D$  is the fractal dimension of the observed averaged relief along the longitudinal direction (it is calculated by the method presented, for example, in [1]),  $D_1$  is the fractal dimension of the boundary of the transverse cut of the conducting area on the surface of the substrate.

The principal control parameters in this model (2) are nanoclusters with fractal dimensions  $D$  and  $D_1$ , which can be obtained in the experiment, and their fractal parameters, which are calculated according to

a certain procedure (in particular, as in a percolation effective medium within the framework of the cellular automaton model [29–31] using images of real nanocluster structures obtained with an atomic force microscope for the nanocluster system under study [21]. In this case, sufficient measurement accuracy ( $D$ ,  $D_1$ ) to the second decimal place is provided, for example, at a length  $L_0 = 100 \mu\text{m}$  with a resolution of 1000 measured points (determines the value of  $l_n$ ).

Therefore, when measuring the electrical resistance in nanostructures, it is necessary to take into account the change in the resistance value depending on the topology of the surface nanolayer obtained in the process of laser deposition [21, 30, 31]. We will return to this in 2.4 of this paper.

Nevertheless, the classical method for estimating the CVC based on Ohm's law, with regard to the methods of fractal geometry, can be applied to nanocluster structures; we will use it with certain restrictions.

Below, we will model such nanocluster structures both in terms of configuration and electrical parameters, presenting a number of results with samples of different nanocluster configurations. Examples of pictures of some real synthesized structures in the obtained samples are shown below.

## 2.1. Conduction paths

Figure 1 shows a diagram of the Lie algorithm we use [2, 32–34], which consists of two stages: current propagation along the conduction path and restoration of its path.

The current propagation is characterized by the fact that, starting from the starting cell, neighboring cells with such an initial cell and located within the Neumann neighborhood are marked with a number one greater than the original one. Path restoration is implemented when, starting from the finish cell, the path is built as a selection of neighboring cells with a label one less than the current one. Thus, the length of the path will correspond to the number of cells of the computational area of which it consists.

The model of the cluster structure being constructed is built within the framework of the DLA (Diffusion Limited Aggregation) approximation with a change in the probability of consolidation of elements forming a cluster (according to the physical process, for example, deposition on a solid surface from a colloid – we are talking about the probabilistic degree of sticking of objects to each other, which is associated with intensity of diffusion in time, in our case in the interval of probabilities  $s[1; 0.01]$  for three

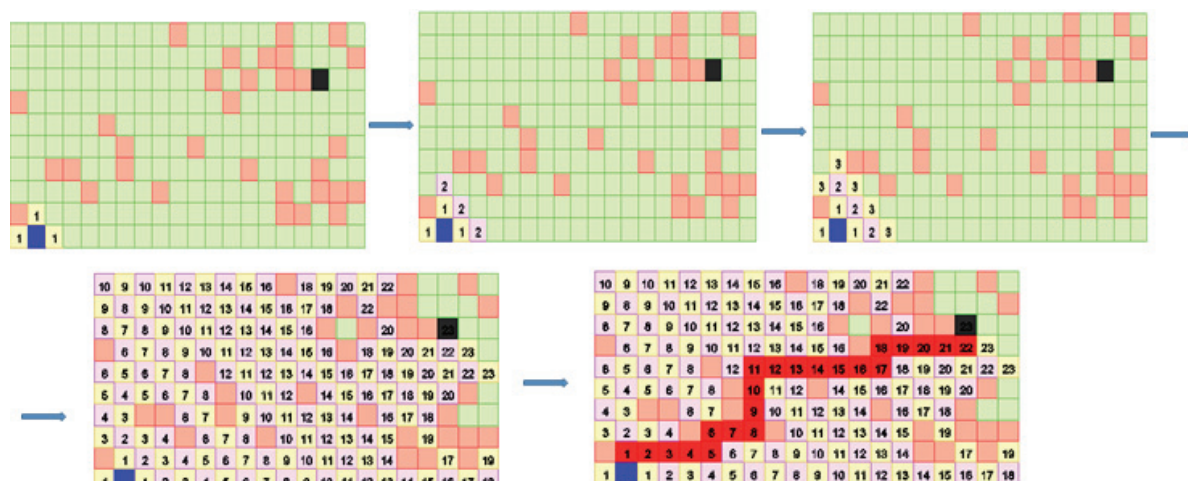


**Fig. 1.** Construction of a conduction path according to the Lee algorithm [33]. Sequential numbers mark the order of propagation from the original cell 1. The final cell formed in this case is labeled 23 here

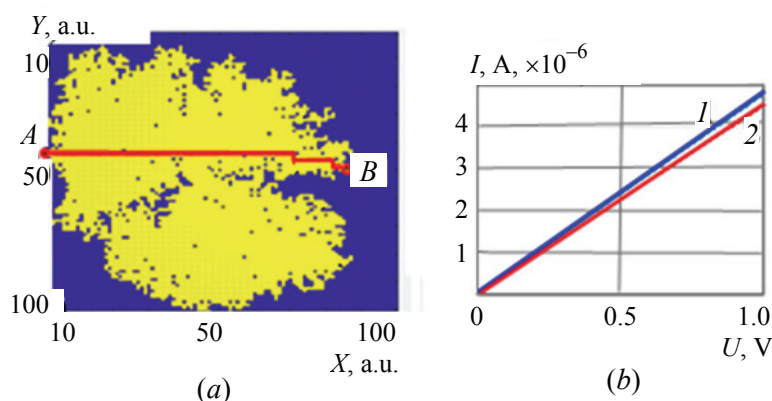
randomly located initial germ particles (granules) with a final surface density with a chosen value of  $5.17 \cdot 10^8 \text{ cm}^{-2}$ , and with a distinguished conduction path (AB) length of 90 rel. un., determined by the Lee algorithm. This path is fixed by the location of the microcontacts in the experimental current measurement circuit.

Figure 2 shows the corresponding CVC at a granule size of 10 nm and an electrical resistivity parameter using the example of a  $\rho_{\text{PbTe}}$  semiconductor film  $\rho_{\text{PbTe}} = 2.32 \cdot 10^7 \text{ (Ohm}\cdot\text{m)}$  [35], with which we performed the experiment.

The specified values allow us to estimate the resistance of the conduction path as  $0.208 \cdot 10^6 \text{ Ohm}$ . The difference between the calculated resistance value and the simulated one is  $\sim 5.5 \%$ . The difference between the estimated CVCs on the basis of the average resistance value from the experimental data and the CVCmodel dependences is about  $5.8 \%$ .

The obtained errors testify to the adequacy of the applied approximation for CVC description.

Figure 3 shows the calculated CVC at a nanocluster size of 20 nm for a model of a well-formed semiconductor nanocluster/island PbTe film in the directional percolation model approximation at a probability  $s = 0.5$  with a surface density of  $5.38 \cdot 10^8 \text{ cm}^{-2}$  on the computational domain with an area of  $50 \times 50$  rel. units (Fig. 3a) with a dedicated conduction path in accordance with the Lee algorithm with a length of 85 rel. units. The comparison was made with an experiment for which the resistivity was  $2.1 \cdot 10^7 \text{ Ohm}\cdot\text{m}$ . For the model structure, the calculated resistance was  $0.17 \cdot 10^6 \text{ Ohm}$ . The difference between the calculated resistance value and the experimentally measured one gives a value of  $10 \%$ . A similar difference was observed between the CVC values.



**Fig. 2.** Model of a PbTe film with a dedicated conduction path (a), CVC of the film for the AB path at a granule size of 10 nm (b): 1 – model dependence; 2 – dependence based on the experimentally estimated average resistance, calculated in the Ohm's law approximation

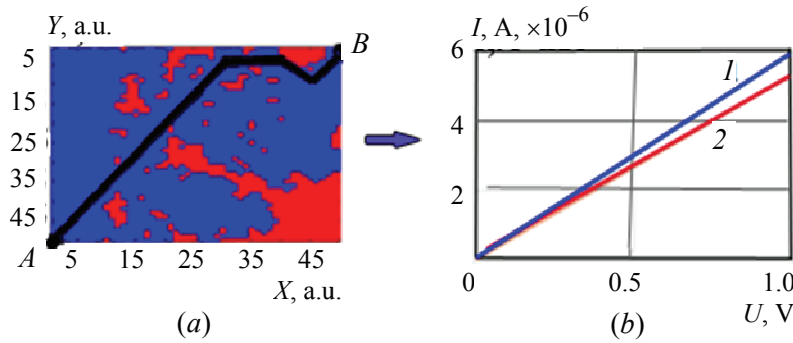


**Fig. 3.** Model of a nanocluster/island PbTe film in the directional percolation approximation (a), its CVC was determined at a grain size of 20 nm: 1 – model dependence; 2 – dependence based on the experimentally estimated average resistance calculated in the Ohm's law approximation (b)

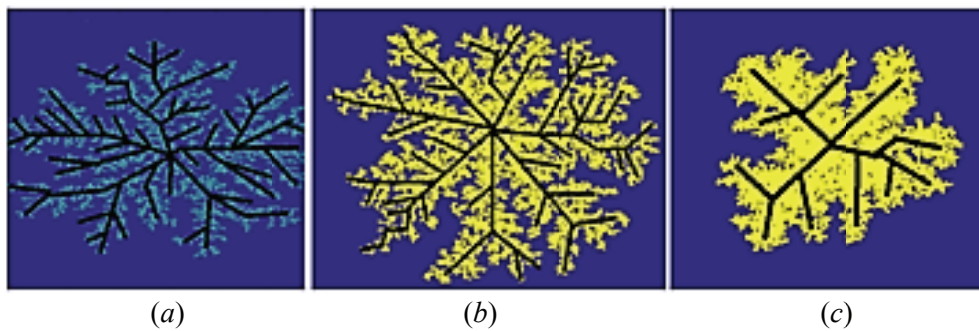


**Fig. 4.** Nanocluster film skeleton at  $s = 1$  (a);  $s = 0.1$  (b);  $s = 0.01$  (c)

Figure 4 shows the obtained models of nanoclusters for different sticking probabilities  $s$ , in which the skeleton of a fractal configuration was previously selected. It tends to complicate its structure with increasing value of  $s$ , and behaves in the same way as the fractal itself that contains it.

## 2.2. Algorithms for calculating electrical conductivity

For nanofilms with a dielectric type of electrical conductivity, with a sparse structure of nanoclusters/islands, we have developed an essentially quantum model of electrical conductivity [30, 36, 37], which implements the CVC estimate taking into account the tunneling effect [30] and charge/electron jumps between islands [37] (they are shown below in Fig. 5).

Then the CVC of the nanofilm is estimated in terms of the sum of the strengths of the currents flowing through the nanoclusters/islands both within them and between them, calculated in accordance with Ohm's law [38]. The resistance of the conduction path in the system of nanoclusters/islands was calculated using the standard formula, taking into account the fact that the length of a possible current path should be the shortest distance between the points of voltage application by microcontacts.

The search for such a distance is carried out according to Dijkstra's algorithm [31].

To determine the direction of such an electrical conduction path between the islands, we used the hopping conductivity approximation, which was implemented as a process of carrier transfer taking into account localized states at a given temperature (it determines the efficiency of electrical conductivity by the thermal activation mechanism). Localized states were understood as states represented by wave functions given in a limited region of space and exponentially decreasing with distance  $r$  outside it:

$$\Psi(r) \sim \exp(-r/a_b), \quad (3)$$

where  $a_b$  is the localization radius, i.e. the size of the cluster.

Thus, hopping conductivity is realized in this model as carrier transfer along localized centers [2].

Such hopping conductivity can be described within the framework of the Miller–Abrahams approach [2, 13, 39], when, based on the localized wave functions of an electron, it becomes possible to estimate the probability of its transition between two neighboring localization centers. Further, by calculating the resulting current, one can estimate the resistance of the electronic junction and reduce the problem to calculating the electrical conductivity of an equivalent network of random resistances.



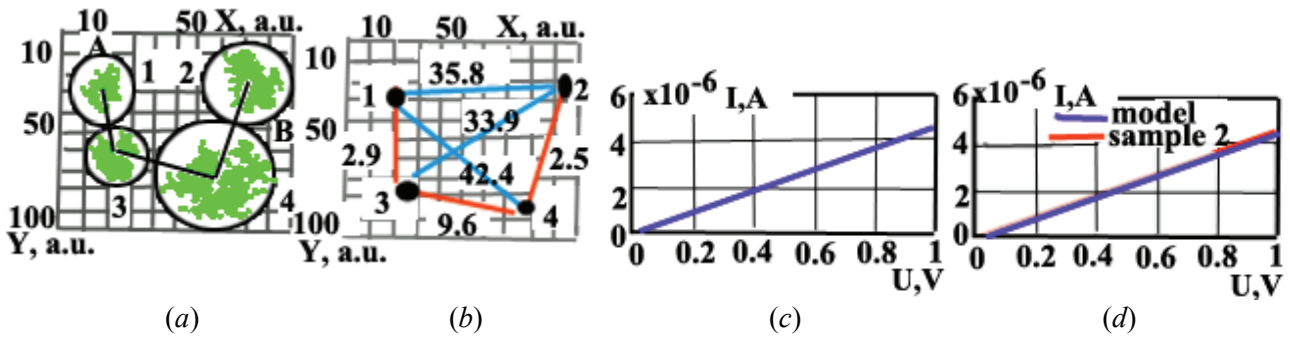


**Fig. 5.** Model of an island PbTe nanofilm of 4 isolated islands and its I-V characteristic at  $T = 300$  K:

*a* – DLA model of the structure with selected minimum coverage circles, *A* and *B* the voltage application points;  
*b* – electron hopping graph; *c* – corresponding CVC; *d* – comparison of the CVC for the sample calculated according to Ohm's law with the simulation results

The resistance connected between a pair of nodes of such a Miller–Abrahams grid [39] has the form:

$$R_{ij} = R_{ij}^0 \exp\left(\frac{2r_{ij}}{a} + \frac{\varepsilon_{ij}}{k_B T}\right), \quad (4)$$

where  $R_{ij}^0$  is the proportionality factor,  $r_{ij}$  is the distance between  $i$  and  $j$  grid nodes,  $a$  is electron or cluster localization radius,  $\varepsilon_{ij}$  is the electron/cluster energy difference at  $i$  and  $j$  nodes,  $k_B$  is Boltzmann's constant,  $T$  is temperature.

The length of the electrical conduction path between nanoclusters/islands  $L_h$  was determined by the Dijkstra algorithm [31, 34] as the shortest distance with the minimum weight.

In this case, the resistance  $R_h$  for the one-electron case is calculated as [40]:

$$R_h = \sum_{i=1}^n R_{ij}, \quad R_{ij} = R_{03} \exp\left(\frac{2w_{ij}}{a} + \frac{\varphi}{k_B T}\right), \quad (5)$$

where  $n$  is the number of edges that make up the conduction path,  $R_{ij}$  is the resistance of the edges included in the conduction path  $L_h$ ;  $R_{03}$  is a constant depending on the radius and character of the distribution of island localization centers,  $w_{ij}$  is the statistical weight of the edge entering the conduction path,  $a$  is the electron localization radius – (hereinafter, for definiteness, we will talk about the electron),  $\varphi$  is the activation energy of conduction.

In this case, for a random distribution of localization centers,  $R_{03}$  has the form:

$$R_{03} = L \frac{\pi \hbar a}{16 q^2} \exp\left(\frac{2}{a N^{1/3}}\right), \quad (6)$$

where  $N$  is the concentration of localization centers,  $q$  is the electron charge,  $\hbar$  is the reduced Planck constant,  $L$  is the scale factor.

Figure 5 shows a model image of a PbTe film with a surface density of nanoclusters characteristic of the real sample 2 we are studying below. For clusters, the circles of the minimum coverage are selected (Fig. 5a), and the corresponding graph (Fig. 5b) of electron hops is constructed, with voltage applied to the points of microcontacts *A* and *B*, taking into account the maximum value of the jump, equal to the localization radius for PbTe with  $a = 50$  nm.

Thus, the total length of the conduction path over islands was 140 rel. units in the model. In absolute terms, taking into account the cell size of the computational region of 10 nm, its digital value is 1400 nm (Fig. 5a). This value corresponds to the resistance  $R_h$ ; inside the nanocluster itself, we denote the resistance by  $R_c$ .

The graph in Fig. 5b shows the shortest distance between islands 1 and 2, the value of which was 15.9 nm. At  $T = 300$  K PbTe parameters:  $\rho = 2.23$  Ohm·m,  $\varphi = 0.31$  eV,  $a = 50$  nm,  $N = 0.15 \cdot 10^{16}$  cm $^{-3}$ ,  $R_h = 0.021 \cdot 10^6$  Ohm, and  $R_c = 0.19 \cdot 10^6$  Ohm. The total resistance is  $R = 0.21 \cdot 10^6$  Ohm.

The magnitude of the calculation error was estimated by the difference  $d$  between the calculated ( $R_m$ ) and average measured ( $R_e$ ) resistances:  $d(R_{me}) = |R_m - R_e|$ . It was 3.8 %.

Figure 5c shows the calculated CVC, taking into account the calculated resistance for the voltage range [0; 1] V at  $s = 1$ . Figure 5d compares the CVC calculated according to Ohm's law for sample 2, taking into account the experimentally measured resistance values, with the calculated current strength



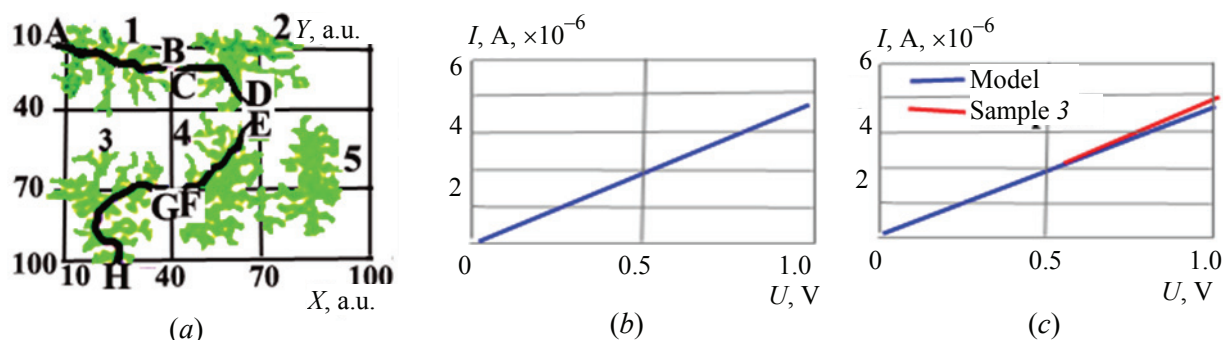


**Fig. 6.** Model of a PbTe island film of 5 isolated islands and its CVC at  $T = 328$  K: DLA model of the structure with the selected shortest distance between the given points A–B (a); CVC (b); the difference between the calculated and measured resistance  $d(R_{me})$  for comparing the CVC characteristics for sample 3 calculated according to Ohm's law with the simulation results (c)

From this figure, we can conclude that the results of experimental measurements and calculations are in satisfactory agreement – their difference does not exceed 10 %.

At  $T \sim 300$  K and parameters corresponding to the cluster structure of PbTe, but for another sample 3 we have:  $R_h = 0.016 \cdot 10^6$  Ohm, and  $R_c = 0.196 \cdot 10^6$  Ohm. Then the total resistance is  $R = 0.212 \cdot 10^6$  Ohm. The results are shown in Fig. 6. Estimating the difference between the results of the experimental measurement of the average resistance and the model calculation for the resistance, we can conclude that it does not exceed 6 %, which also indicates a satisfactory degree of agreement between the simulation results and experimental measurements.

Thus, we can conclude that the use of the electrical conductivity model based on the formation of a conductivity cluster, taking into account tunneling and the hopping mechanism between cluster islands, makes it possible to describe the experimentally observed phenomena for island/nanocluster nanofilms of various elemental compositions (we considered this approach and used it for different substances: Au, Ag and their complexes, PbTe, etc.) [1, 26].

### 2.3. Local fields and amplification factors for electrical conductivity

In a dense ensemble of nanoparticles on the surface of a semiconductor with a static permittivity  $\epsilon_S$  (for PbTe  $\epsilon_S \sim 400$  at  $T = 296$  K [41]), the local electrostatic field  $E_i$  in such a cluster system, due to inhomogeneities and collective effects, can greatly exceed the external applied field  $E_e$  due to the localization of the electric field at the sharp boundaries of the tips of inhomogeneities. This is the basis in optics, for example, of the effect of a sharp increase in the intensity of Raman scattering of light

by molecules on a surface (Surface Enhanced Raman Scattering – SERS) for surface rough metal media (see, for example, [1, 2, 18, 19]). The physics of this phenomenon is associated with the occurrence of localized surface plasmon resonances for certain wavelengths, depending on the surface material. However, geometric factors are of fundamental importance – the size of such local protrusions with their boundary conditions, as well as the density of these objects. But in electrophysics, everything is more complicated due to the ongoing averaging of parameters along the streamline, in particular, with a statistical spread of roughness heights and a finite size of the tip of the measuring microcontact/needle.

When considering this effect, an ensemble of nanoclusters on the surface of a semiconductor will be modeled by cylindrical nanoprotusions that allow an analytical solution, with a static permittivity  $\epsilon_S$ , a height of  $2b$ , and a diameter of  $2a$ .

If the condition on these key parameters  $b \ll a$  is satisfied, then it is unfavorable in terms of strengthening the local field, since such a structure is practically flat.

Within the framework of this model, it is considered that the protrusions are randomly distributed over the surface with a density of  $n$  [ $\text{cm}^{-2}$ ], and they are under the influence of an external lateral electrostatic field  $E_e$ .

It is physically clear that the field amplification factor  $G$  at an isolated inhomogeneity tip can be estimated as  $G \sim b/a$  [42]. However, the local field inside the selected nanoprotusion is formed as the sum of the nanocluster field violating the cylindrical symmetry (we call the effect of such a defect by the term depolarization effect)  $E_L$ , and the field  $E_\beta$ , acting on the selected nanoprotusion from the surrounding objects:

$$E_i = E_e - E_L + E_\beta, \quad (7)$$

where  $E_L = \frac{4\pi Ld}{V}$ ,  $L$  is the depolarization factor of the shape of a cylindrical nanocluster,  $d$  is the dipole moment,  $V = 2\pi a^2 b$  is its volume,  $E_\beta = \frac{4\pi\beta d}{V}$ ,  $\beta$  is the acting field factor [43]. In this approximation, we do not take into account the difference in the parameters of the medium in terms of scale for a monolithic sample and a micronanostructured one.

Given that

$$\frac{d}{V} = \frac{(\varepsilon_S - 1)E_i}{4\pi}, \quad (8)$$

we obtain an amplification of the local field inside the nanocluster [42, 44]:

$$E_i = \frac{E_e}{[1 - (\varepsilon_S - 1)(\beta - L)]} = GE_e, \quad (9)$$

where  $G = 1/[1 - (\varepsilon_S - 1)(\beta - L)]$  is field enhancement coefficient inside the nanoprotusion (if  $\beta > 1$ ).

To estimate  $\beta$ , we calculate the field created inside a selected cylindrical nanoprotusion (with radius vector  $r$ ) by the dipoles surrounding it. The dipole  $d$ , with radius-vector  $r$ , creates a field in the center of the base of the selected cylinder  $E_d = d/r^3$ . Summing over all dipoles, except for the selected one, we have for the total field of dipoles in the center of the selected quasi-planar nanocluster:

$$E_d = n \int_0^{2\pi} \int_0^\infty d\varphi \int_a^\infty r \left( \frac{d}{r^3} \right) dr = \frac{d2\pi n}{a}. \quad (10)$$

From the equality  $4\pi\beta d/V = E_d$  we find the estimate of the factor of the acting electrostatic field  $\beta = \pi nab$ .

The depolarization factor of the cylinder in the case of an electrostatic field is determined numerically [43]. It shows that the depolarization factor of the cylinder practically coincides with the depolarization factor of the ellipsoid with the same aspect ratio for its axes  $b/a$ .

So, for an ellipsoid, under the condition  $a \gg b$  depolarization can be represented as:

$$L = \left( \frac{b}{2a} \right) \arctg \left( \frac{a}{b} \right) < \left( \frac{b}{a} \right) \left( \frac{\pi}{4} \right) \quad (11)$$

and the acting field factor, using the relation  $n = 1/(\pi a^2)$ , has the form:

$$\beta = \pi nab = \frac{b}{a} > \left( \frac{b}{a} \right). \quad (12)$$

Comparing the obtained expressions for  $L$  and  $\beta$ , respectively (11) and (12), we can conclude that in the electrostatic case under consideration, a situation is possible when  $\beta > L$ . If there is a wide spread in the aspect ratio of nanoclusters in their ensemble, the presence of a subensemble with  $\beta \sim L$  is possible. Then from (9) it follows that in the case under consideration with  $\varepsilon_S \gg 1$ , it is possible, in principle, to increase by orders of magnitude ( $G \gg 1$ ) the electrostatic field  $E_i$  inside the nanocluster compared to the external field  $E_e$ , since the denominator in relation (9) can become close to zero for  $\beta \gtrsim L$ , and a condition arises in the denominator for the expression for  $G$  when  $(\varepsilon_S - 1)(\beta - L) \leq 1$ .

However, the very value of the density  $n$  and the shape of the inhomogeneity tip are also important [42]. In particular, for large  $n$ , the field can be screened from neighboring nanoclusters with different parameters.

We make such an estimate of the amplification factor  $G$  in the above approximation depending on the density of nanoclusters on the sample surface ( $n$ ). We define the dependence of the nanoprotusion radius on the density of nanoclusters as  $a(n) = 1/\sqrt{\pi n}$ . Then, taking into account relations (9) and (11), the dependence of the gain on the density of nanoclusters will have the form:

$$G(n) = \frac{1}{1 - (\varepsilon_S - 1) \left( \frac{b}{a(n)} - \frac{b}{a(n)} \arctg \left( \frac{a(n)}{b} \right) \right)}. \quad (13)$$

Then for the values of  $n$  and the value of  $\varepsilon_S \sim 400$  at  $T = 295$  K for the parameter  $b = 100$  nm in the approximation of cylindrical nanoprotusions, the calculated field enhancement does not exceed 1.56, i.e. 50 % of the average value for the longitudinal direction (Fig. 7a) and a value of 1.179 or 17 % of the average value for the transverse direction (Fig. 7b). The modeling error turned out to be about 3.8 % for the longitudinal direction and 1.6 % for the transverse one. Such error values testify to the satisfactory adequacy of the proposed model.

Thus, within the framework of the model used, we see that the amplification factor  $G$  for a semiconductor material (in our case, this is PbTe) is significantly inferior to its values, for example, for noble metals (it is  $\sim 1000$  for them). But what

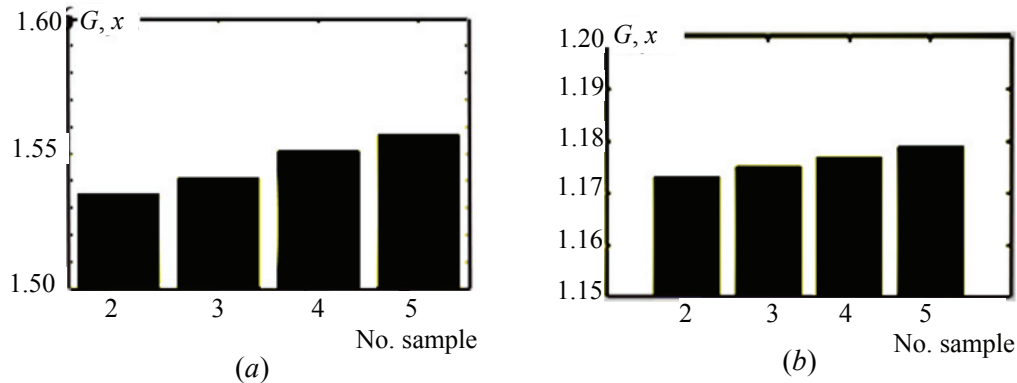


**Fig. 7.** Calculated value of the field strength gain according to the model of the system of nanoprotusions for samples 2–5 with different surface topology: *a* – longitudinal direction; *b* – transverse direction

is important for us now is mainly methodological approaches for carrying out calculations. For SERS-activation of semiconductor materials, complex amplification mechanisms are implemented, which are determined by various defects and vacancies in them, as well as by the composition of the studied molecules. This requires modification of the parameters, in particular, in relation (13), with a significant decrease in the value of its denominator. However, such an assessment of these factors is beyond the scope of this paper. But, on the other hand, our estimates indicate the possible conditions for using the approaches of macroscopic electrodynamics of monolithic samples for the considered nanostructured objects, in our case, for PbTe. This is important in practice when analyzing certain problems of nanoelectronics and nanophotonics.

#### 2.4. Experimental methodology

To study the electrical conductivity of nanocluster/island nanofilms, their electrical resistance is analyzed. At present, there are many methods for measuring the resistivity of metal and semiconductor island nanomaterials and structures [44–46].

The main characteristics of the most popular and convenient methods for determining the resistivity of nanostructures are summarized in Table 1. Analyzing the above table, we can conclude that the four-probe method is most suitable for measuring the nanocluster/island nanofilms obtained by us.

Experimental studies of the electrophysical properties of the nanocluster/island nanofilms obtained by us were realized through the measurement of their CVC. In this case, the analysis was carried out using a four-probe circuit with a linear arrangement of contacts (Fig. 8) [45–47]: two extreme contacts 1 and 4 provided a direct current supply  $I$  using a stabilized power source and were located at the same distance from each other,

$S_1 + S_2 + S_3 = (6 \pm 0.01)$  mm. The inner probes, 2 and 3, were conducting needles of an atomic force microscope with a radius of curvature of 100 nm. The pressing force of the probe was about 1 N.

The required current was set on the source, and the corresponding voltage was taken from the voltmeter. To carry out temperature measurements, the entire circuit was assembled in a vacuum thermal chamber with the possibility of reaching a pressure of  $10^{-3}$  Torr and heating the sample to 100 °C.

**Table 1.** Characteristics of methods for measuring the resistivity of semiconductor structures

Method	Error, %	Locality	Range $\rho$ , Ohm·cm
Four-probe	1–5	10–50 $\mu$ m	$10^{-4} - 5 \cdot 10^3$
Spreading resistance	5–20	10 $\mu$ m	$10^{-3} - 5 \cdot 10^2$
Contactless	10–20	1 mm	$5 - 10^2$

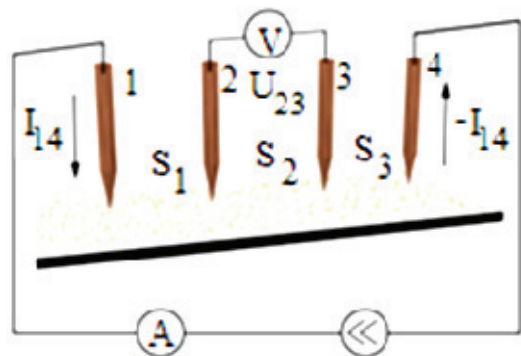


**Fig. 8.** Schematic representation of a 4-probe circuit

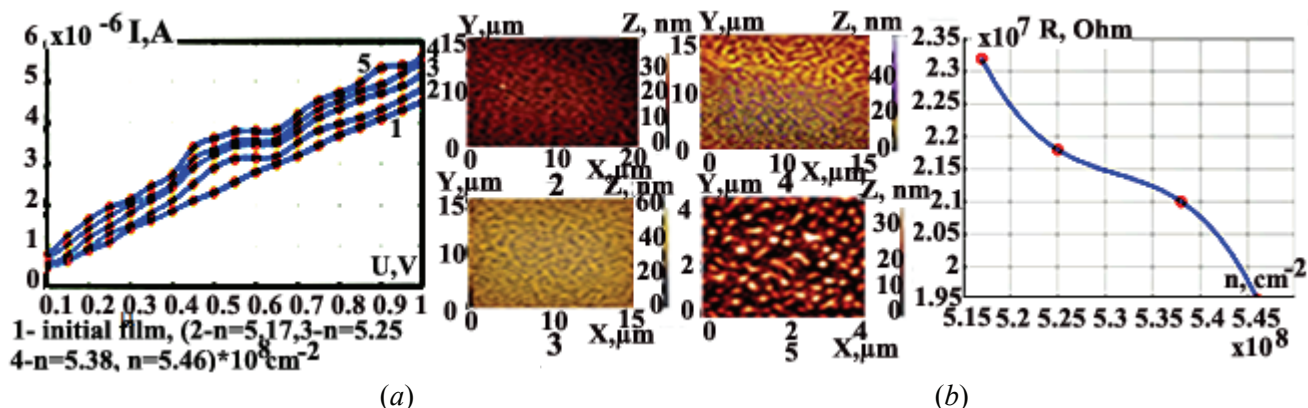


Fig. 9. *a* – CVCs (shown on the left)  $I(U)$  for the original ( $I$ ) and nanommodified (2–5) nanocluster/island PbTe thin films (their AFM images, which were obtained using NT-MDT NTEGRA, are shown on the right) – the surface density of nanoobjects is indicated directly by the curves; *b* – experimental dependence of electrical resistance on the surface density of used nanoobjects [51]

### 3. Results and Discussion

#### 3.1. Current-voltage characteristics and conduction mechanisms

The current-voltage characteristics of the original and nanommodified PbTe films are shown in Fig. 9. The CVC measurement in the experiment was carried out at room temperature ( $23 \pm 2$ ) °C. The voltage varied from 0.1 to 1 V. The resistance value in the studied range was about 107 Ohm. To average the result, 8–10 points on the sample surface were used [48, 49]. The resulting dependence was approximated by cubic splines for 100 points implemented in the MATLAB environment [50]. The current strength was about  $10^{-6}$  A. The current strength measurement error was 0.5% of its average value. CVC measurements were made in the longitudinal and transverse directions, which made it possible to show the dependence of the current on the topology of the sample under study (Fig. 9) [51].

It is clear from Fig. 9a (straight line  $I$ ), that in the absence of an ensemble of nanodots/nanoclusters on the film surface, its CVC has a linear character, in accordance with Ohm's law, with the dependence of the current density  $J$  on the external applied field  $E_e$  [49]:

$$J(E_e) = \sigma E_e, \quad (14)$$

where  $\sigma$  is electrical conductivity.

Analyzing Fig. 9a, we can conclude that the nanomodification of the surface leads to the appearance of characteristic features of the CVC for PbTe: an increase in its slope and the appearance of a pronounced local maximum. However, the dependence of CVC on average demonstrates a linear character in the voltage intervals (0.1–0.4) V and (0.65–1) V, and for the average voltage values in the

interval (0.4–0.65) V, a resonant current surge was observed. The magnitude of this surge was about 50 % of the average value for the longitudinal direction: the maximum value of the CVC surge is  $0.5 \cdot 10^{-6}$  A. In the case of the transverse direction, the maximum value of such a surge was about 16 % –  $0.15 \cdot 10^{-6}$  A. This can be caused by a higher density of cluster nanogranules in the longitudinal direction compared to the transverse one, which amounted to an average ratio of their densities of about 5.5 (Fig. 9b).

In this aspect, 1D structures are a typical example of an increase in electrical conductivity due to the dominant polarizability along one preferred direction. An illustrative example of such an effect is demonstrated by our experiments with a 1D carbon structure (LLCC) [4, 5, 8, 10, 11].

This demonstration curve for the CVCs obtained experimentally [10, 11] for an LLCC system in combination with Au–C–Au atoms is shown in Fig. 10 for a thin film 30 nm thick. An increase in electrical conductivity compared to the usual Ohm's law occurs due to the high polarizability of the 1D LLCC structure along the preferred direction [10, 11].

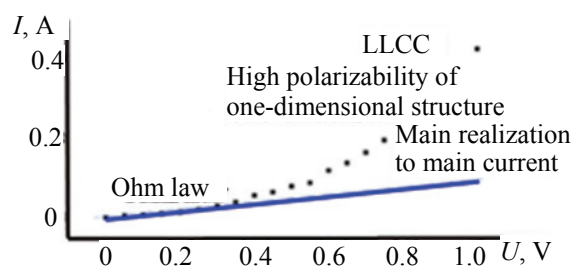


Fig. 10. Current-voltage characteristics for carbyne in the Au–C–Au system in a thin film on a solid surface with a thickness of 30 nm [10, 11]



In addition, the appearance of a resonant burst, as well as an increase in the CVC slope, can be considered as a result of the participation of weakly and strongly bound electrons in the surface electrical conductivity, which are initially at the size quantization levels in nanoclusters, taking into account the enhancement of the local field [50]. Thus, we assume that electrons are in a potential well (the standard quantum model of a cluster) [19] with a width of  $2a$  and a depth of  $P$ , and occupy energy levels of size quantization. In this case, the uppermost

level ( $N$ th) of the filled levels has the  $\varepsilon_N = \frac{N^2 \pi^2 \hbar^2}{8m^* a^2}$ ,

energy, where  $m^*$  is the effective electron mass,  $\hbar$  is the constant Planck, and is separated from the top of the potential well by the energy distance  $\Delta_N = P - \varepsilon_N \gg k_B T$ ,  $T$  is the temperature,  $k_B$  is the Boltzmann constant. Under these conditions, a spontaneous transition of bound electrons to a free state (to the conduction band) at ordinary temperature is unlikely. However, due to the cluster structure, the presence of a local field  $E_i$ , even without an external applied field  $E_e$ , reduces the effective energy barrier depth for an electron by  $eE_i 2a$ . In this case, thermal ejection of an electron from the upper energy level from the well becomes possible [51].

Comparing the CVC for different films – a continuous PbTe film (the initial one in Fig. 9 and a nanocluster/island thin PbTe film, samples 2–5 in Fig. 9), we can conclude that the electrical conductive properties of the island structure have their own significant features. Therefore, the use of semiconductor nanostructured thin-film cluster structures in certain cases for a number of tasks is more preferable than solid films.

To elucidate the mechanism of electrical conductivity, the electrical resistance of the films was studied as a function of temperature in the range from 20 to 100 °C [51, 52]. Figure 11 shows the dependences of the natural logarithm of the resistance  $R$  on the reciprocal temperature  $1/T$ . Curves R1 – R5 correspond to films with different density of nanoclusters/dots on the surface (according to the data for samples 1–5 in Fig. 9).

As can be seen from Fig. 11, in the range from 20 to 85 °C, the electrical conductivity has a tunneling character – it does not depend on temperature. At temperatures above 85 °C, the behavior of electrical conductivity changes, which is caused by the manifestation of the thermal activation effect; the character of electrical conductivity becomes predominantly hopping [10, 51, 52].

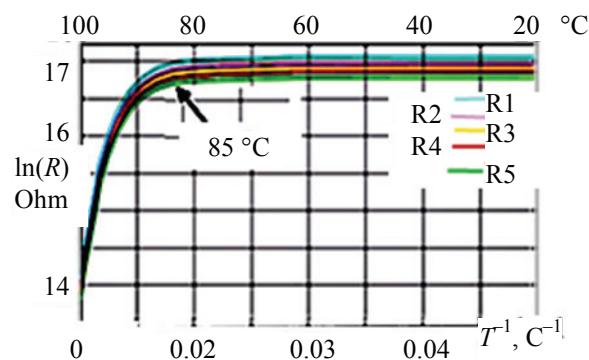


**Fig. 11.** Temperature dependence of the natural logarithm of the resistance  $\ln(R)$  of films obtained under various deposition modes (see Fig. 9) with the same activation energy for all samples, equal to 0.3 eV [51, 52]

To estimate the experimental dependence of resistance  $R$  on temperature  $T$ , the relation [2, 13] is applicable:

$$R \approx R_0 + R_1 \exp\left(\frac{\varphi}{k_B T}\right), \quad (14)$$

where  $k_B$  is Boltzmann constant,  $\varphi$  is the activation energy.

The first term in (14),  $R_0$  is due to the temperature-independent tunneling effect, and the second one –  $R_1$  is determined by thermally activated electron jumps. The thermal activation energy of hops between islands turns out to be significantly lower than the electron work function for this material in a bulk/monolithic sample, which is due to the effect of the granular structure on the substrate [2]. This allows us to speak about the possibility of creating effective elements of nanoelectronics and nanophotonics by analogy with quantum cascade devices [12].

### 3.2. The role of photoconductivity

For the electrophysics of thin films with a fractal structure, it is necessary to take into account the role of photoelectric conductivity, which depends on the spectral characteristics of the external radiation surrounding the sample. We simulated this process for the case of sample illumination with green laser radiation. In this case, the tunnel photocurrent naturally increases depending on the degree of illumination [2].

To evaluate the obtained dependencies, we used the apparatus of mathematical modeling in the MATLAB environment. The current-voltage characteristics were modeled in the Schottky

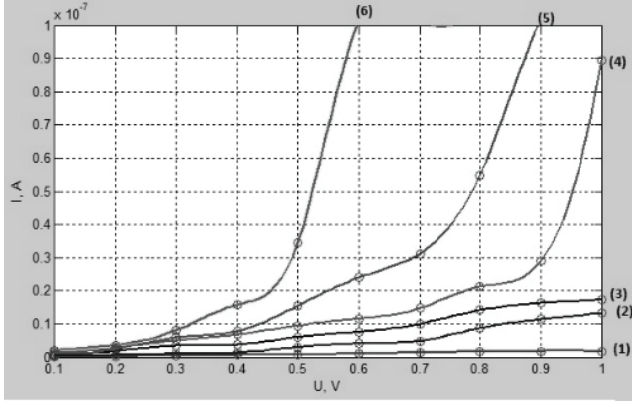


**Fig. 12.** Current-voltage characteristics of the tunnel current at different degrees of illumination:

$I$  – dark current, and also at different values of  $\gamma$  (%):  
2 – 5 %; 3 – 25 %; 4 – 50 %; 5 – 75 %; 6 – 100 %

photodiode approximation as the sum of the dark current  $I_d$  of the photocurrent  $I_{ph}$  [2, 13, 32]:

$$I = I_d + I_{ph}. \quad (15)$$

The dark current was estimated as:

$$I_d = I_0 \exp(qU/Nkt) - 1, \quad (16)$$

where  $I_0 = RA^* T \exp(-\phi/kT)$ ,  $q$  is the electron charge,  $\phi$  is the potential barrier,  $U$  is voltage,  $k_B$  is Boltzmann constant,  $T$  is temperature,  $A^*$  is Richardson constant,  $S$  is contact area,  $R$  is the electron reflection coefficient,  $N$  is the structure ideality coefficient. The sample temperature was assumed to be 293 K, the contact area was  $10^{-16} \pi \text{ (m}^2\text{)}$ , i.e. its radius was assumed to be 10 nm. The photocurrent was estimated as [53]:

$$I_{ph} = (qF\mu\tau/d^2)\gamma, \quad (17)$$

where  $F = (2qU/m_e)^{1/2}$  is the velocity of free electrons,  $\mu = (F U)/d$  is mobility,  $d$  is the distance from the nanofilm to the probe (1 nm),  $m_e$  is the electron mass,  $\tau$  is the lifetime ( $10^{-10}$  s),  $\gamma$  is the degree of illumination: it was a fitting factor and was estimated as  $\gamma = I_{100}/I_\gamma$ , where  $I_{100}$  is the measured current at 100 % illumination,  $I_\gamma$  is the measured current at illumination in  $\gamma$  %.

Figure 12 shows the model CVCs of the tunnel current in the case of different illumination intensity for the voltage range from 0.1 to 1 V, which we built in MATLAB using spline approximation.

For the proposed model, it was possible to achieve an error of the order of  $10^{-2}$ , which indicates a satisfactory degree of adequacy and allows, in a first approximation, to estimate the photoelectric properties of the structures obtained. This is of particular interest for various applications.

### 3.3. Temperature field calculation

Next, we briefly dwell on the calculation of the temperature field  $T$  that arises when scanning a laser beam of size  $a$  during the deposition of nanoclusters from a colloid on a solid surface under conditions of a moving laser source of intensity  $I$  over the sample surface using the following relationship [2, 18, 19]:

$$T(x, y, z, t) = \int \int_{-\infty}^{\infty} AI(x', y') W(x, y, z, x', y', v) dx' dy', \quad (18)$$

where the following parameters are indicated:

$$W(x, y, z, x', y', v) = \frac{1}{2\pi KR} \exp\left(-\frac{j}{2a}(x - x' + R)\right),$$

$$R = \sqrt{x^2 + y^2 + z^2},$$

coefficient  $A$  is the absorbance of the material,  $K$  is the thermal conductivity ( $\text{W} \cdot (\text{m} \cdot \text{K})^{-1}$ ),  $j = K/\rho c_p$  is the thermal diffusivity ( $\text{m}^2 \cdot \text{s}^{-1}$ ) of the material,  $v$  is the scanning speed of the laser beam ( $\text{m} \cdot \text{s}^{-1}$ ),  $\rho$  is the density ( $\text{kg} \cdot \text{m}^{-3}$ ) of the sample substance,  $c_p$  is the specific heat capacity. Expression (18) was calculated using the fast Fourier transform (FFT) [54].

These calculations of the temperature field distribution on the surface of a target (sample in the form of a plate) made of lead telluride [49, 55] were carried out for the following parameters:  $A = 0.01$ ,  $K = 2.3 \text{ W} \cdot (\text{m} \cdot \text{K})^{-1}$ ,  $\rho = 8200 \text{ kg} \cdot \text{m}^{-3}$ ,  $c_p = 151 \text{ J} \cdot (\text{kg} \cdot \text{K})^{-1}$  on a model square calculation area with a size of 400  $\mu\text{m}$ .

For example, the results of calculations for the case of laser exposure with a power of  $P = 8 \text{ W}$  at beam diameters  $d_{\text{beam}} = 30 \mu\text{m}$  and  $d_{\text{beam}} = 100 \mu\text{m}$  at a scanning speed  $v_{\text{sc}} = 80 \mu\text{m} \cdot \text{s}^{-1}$  of the laser beam over the surface are shown in Fig. 13. The laser beam was applied to the center of the computational area. The initial temperature of the sample plate was 300 K.

Figure 13 shows that in the case of a laser spot diameter on the sample surface of 30  $\mu\text{m}$ , the maximum temperature at the center of the spot is  $(776 \pm 0.2) \text{ K}$ , which is much lower than the melting point of lead telluride (1190 K). With an increase in the beam diameter, the temperature field expands significantly with a simultaneous significant decrease in temperature to  $(420 \pm 0.2) \text{ K}$  at the center of the laser spot. The temperature distribution is asymmetric on the plane and is elongated in the direction of the laser beam: the target material in front of the moving source ( $x > 0$ ) is heated weakly.

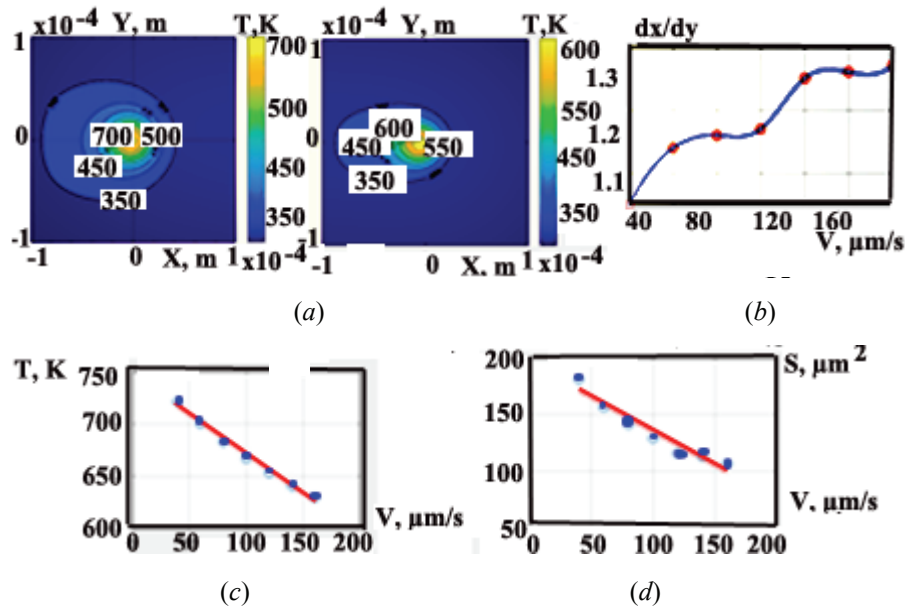


**Fig. 13.** *a* – Effect of the laser beam velocity at its scanning of the sample surface on the temperature field at the laser power  $P = 7$  W,  $d_{\text{beam}} = 50$   $\mu\text{m}$ : temperature field in the case of a velocity of 40  $\mu\text{m}\cdot\text{s}^{-1}$  (left) and 160  $\mu\text{m}\cdot\text{s}^{-1}$  (right);  
*b* – the dependence of the eccentricity of the temperature area on the velocity in the approximation by splines;  
*c* – dependence of the maximum heating temperature on the velocity;  
*d* – dependence of the area of the heated region on the velocity

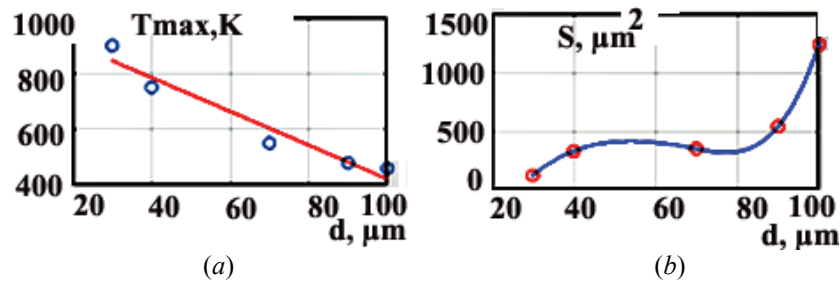


**Fig. 14.** Influence of the laser beam parameters on the realized surface temperature area: *a* – dependence of the maximum temperature  $T_{\text{max}}$  on the laser beam diameter  $d$ ; *b* – dependence on the beam diameter for the area of heating regions with the same temperature 350 K

The characteristic heating region (Fig. 13) has a value on the order of the laser beam cross-sectional area on the sample surface. Its shape differs from round and is elongated in the direction of movement of the radiation source. The temperature of the heating region decays slightly, and the length of the elongated part of the heating region does not exceed a quarter of the length of the heating region.

In the case of an increase in  $d_{\text{beam}}$  at fixed power  $P = 7$  W,  $v_{\text{sc}} = 80$   $\mu\text{m}\cdot\text{s}^{-1}$ , the following modes are realized: the maximum temperature  $T_{\text{max}}$  decreases in accordance with the following approximation:  $T_{\text{max}}(d_{\text{beam}}) = -0.0061d_{\text{beam}} + 1.0279$  (Fig. 14a), and the heated area  $S$  increases significantly (Fig. 14b).

#### 4. Conclusion

The thin-film solid-surface nanocluster structures of various configurations with cardinally controlled electrophysical characteristics considered in this article indicate the possibility of developing and creating nanoelectronics and photonics elements and systems with specified/required functional characteristics based on new physical principles.

Although we discussed only electrophysics, such a transformation of properties also applies to other characteristics, in particular, to optical ones (see, for example, the review in [1]). To date, a number of priority areas have already been formulated in this area. Among them are the following.

First, the presence of lateral fractal-type segments of different structures can, firstly, link various 1D current transport trajectories into a single ensemble [29] and increase (by analogy with a conventional conductor) the effective cross section in the form of such a bundle of trajectories (compare with [56]). Secondly, to lead to strong local electric fields at the "tips" of nanoclusters with sharp boundaries with the implementation of the effects of hopping conductivity and/or phenomena with a Coulomb gap, and/or with the thermally activated nature of electrical conductivity [28, 52, 57]. Third, they can be considered as a model of a medium by analogy with quasicrystals and structures with superlattices with translational symmetry [58].

Second, consideration of the formation of closed 2D structures of various configurations with edge channels on a percolation grid makes it possible to implement various controlled modes of electrical conductivity with different mechanisms in synthesized fractal cluster systems with a controlled electrical resistance over a wide range [28, 53].

Third, the quantum analysis of electrophysics for such objects, taking into account quantum fluctuations within the framework of the ideology of quantum phase transitions, makes it possible to substantiate the controlled obtaining in an experiment under normal conditions of exotic effects considered until now [59, 60] in electrical conductivity, which are realized under extreme conditions [10, 11, 15, 50]. First of all, this concerns one-dimensional 1D systems and their transformation in 2D and 3D structures of complex configuration for carbon materials both in carbon objects pure in elemental composition and in their various compositions, in particular, with noble metals [61–66].

A unique basis for successes and achievements in this field has already been created thanks to the solution of the problems of synthesizing a large class of carbon compounds with outstanding results even on an industrial scale [67–73].

All this can be very important for various topologically modified structures with superconducting phase states in carbon-containing compositions with different configurations and elements. This should determine the corresponding trends and trends in the increase in electrical conductivity, and will make it possible to predict the manifestation of such fundamental properties, on the basis of which the discussed real prototypes of hybrid topological electrophysical objects can be created on the basis of new physical principles [66]. Fundamental success here can be predicted for the future, taking into

account modern technological capabilities for the synthesis of carbon-containing systems of various dimensions (from 0D to 3D) and their complexes. Progress in this area is very dynamic, especially in terms of developing technology and equipment for the industrial production of nanostructured carbon materials of various compositions in complex systems for various purposes [67–73]. Of great importance here are studies in conglomerates with scandium, which, as shown in a recent paper [74].

The considered technologies using laser ablation are universal, they do not require expensive vacuum equipment used in epitaxial electronics, and constitute a promising area of printed electronics with controlled functional characteristics of synthesized objects, including nanotopological electrophysics and optics/photonics. It is precisely the controlled configuration of similar samples with surface topology of different dimensions and controlled elemental composition [41] that makes it possible to determine the physical principles and tendencies towards achieving superconducting states in micronanosystems for possible use in various CVC devices and new generation systems, including nanoelectronics and nanophotonics [10, 11, 75–103].

## 5. Additional materials (Appendix) Models of controlled synthesis of fractal structures

Without dwelling on the model images of the formed clusters and their structure (cf. Fig. 9) in dynamics, we only note once again that the process depends on the sticking probability parameter  $s$  of clusters to each other, which makes it possible to take into account the intensity of the thermal diffusion coefficient in the simulated system. Its value significantly affects the shape of nanoclusters/islands of a nanofilm: at low values, clusters with high degrees of filling are generated, and at large values, with low degrees of filling. The degree of branching of the structure (value and number of branches), expressed by the values of the fractal dimension characterizing the inhomogeneity, is proportional to the sticking probability (see Fig. A.1 below).

Thus, the number of main branches  $N_{bm}$  of a single cluster can be estimated depending on the fractal dimension  $D_f$  based on the relation:

$$N_{bm}(D_f) = \left\lfloor \frac{2}{D_f - 1} + 1 \right\rfloor + 1, \quad (\text{A.1})$$

where two vertical lines  $\lfloor \cdot \rfloor$  mean taking the whole part of the number.



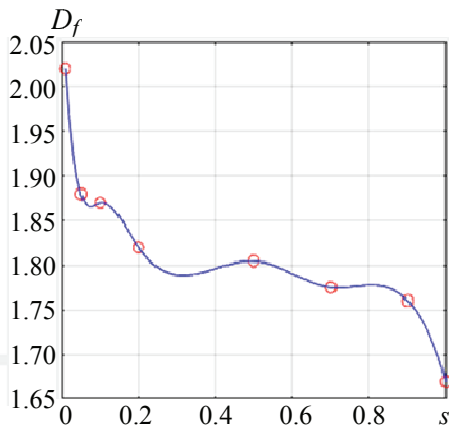


**Fig. A.1.** Dependence of the fractal dimension ( $D_f$ ) on the sticking probability value ( $s$ ) taking into account the cubic spline approximation of the MATLAB programming

The performed computational experiments and their statistical processing have shown that the DLA model of aggregation with limited diffusion [50] makes it possible to obtain fractal clusters with dimensions ranging from 1.67 to  $(2.02 \pm 0.03)$  by varying the sticking probability  $s$  in the range of values  $[1; 0.01]$  (Fig. A.1).

In turn, the temperature dependence for the fractal dimension is determined by the relation:

$$D_f(T) \approx A_0 T^\alpha, \quad (\text{A.2})$$

where  $A_0$  and  $\alpha$  are proportionality coefficients within a certain calculation procedure [1, 55].

The anisotropy of the experimentally obtained fractal nanocluster configurations in the model used by us for the computational domain can be specified by determining non-equiprobable single random displacements of a particle during its diffusion wandering. This method of taking into account the anisotropy makes it possible to set the direction of diffusion of nanoparticles into the region of laser

heating as an increased probability of random displacements.

Specific values of  $D_f$  should be substituted into the ratio (A.2) for electrical resistance.

Thus, Fig. A.2 shows the results of the calculation within the framework of the DLA scheme, presented in Section 2, in the case of non-equiprobable displacements from a single initial nucleus located, for example, in the center of the computational domain.

Figure A.2 shows that the growth of the cluster is realized in directions with maximum probabilities of single displacements. In this case, the area of influence of laser radiation is located to the right of the center for the model from Fig. A2a, at the top on the right diagonal for the model from Fig. A2b, at the bottom on the left diagonal for the model from Fig. A2c.

The anisotropy of the computational domain can also be specified through the definition of the temperature field. Then, having a temperature distribution in the case of a flat substrate in the form of a system of isothermal regions, it becomes possible to estimate the sticking probability for a wandering particle when it enters one or another isothermal region.

We determine the temperature field directly for the PbTe sample. Since the length of thermal diffusion along the normal to the surface during the passage of the laser beam ( $\sim 1$  mm) was estimated to be much larger than the absorption length of laser radiation ( $\sim 10$   $\mu\text{m}$ ), the heat source was considered to be surface [18, 67]. In addition, the radiation source had a sufficiently high speed of movement, so the heat losses can be neglected and the flat case can be considered without taking into account heat fluxes. Also, since the thickness of the heated layer is much less than the thickness of the epitaxial film, the influence of the substrate can be neglected.

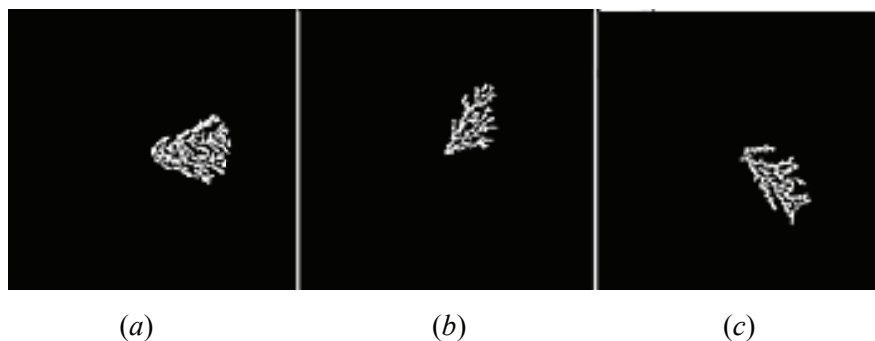


**Fig. A.2.** Model images of clusters at  $s=1$  in the case of different non-equiprobable displacements:  
 a – the probabilities of displacement up and down are the same in value 0.25, to the left 0.05, to the right 0.45;  
 b – up 0.45, down 0.05, left 0.05, right 0.45; c – up 0.03, down 0.22, left 0.05, right 0.45

Thus, our model has the following assumptions [68]:

(1) a plane case on a square computational domain is considered;

(2) heat losses and the effect of the substrate on the temperature field are not taken into account;

(3) boundary conditions are given by I-type conditions: a constant temperature is maintained at the boundaries;

(4) the quasi-stationary case is considered.

In this approximation, we considered the models of fractal nanocluster systems in Section 2, for which we analyzed the electrophysical characteristics for thin films on a solid surface in this article. At the same time, carbon-containing compositions synthesized of various types and their configurations of various dimensions, especially low-dimensional ones, exhibiting quantum properties, as well as demonstrating modes of nonlinear dynamics in localized structures with the implementation of topological phase transitions of various nature, are of particular fundamental importance both in fundamental and applied aspects.

In general, it should be emphasized that a large volume of scientific, scientific, technical and technological and industrial publications in this area determines the unique possibilities for obtaining and controlling the functional characteristics of various similar structures and hybrid systems based on them using powerful methods of mathematical and computer modeling, situational predictive modeling with prediction of obtaining the required characteristics and results in various applications, both technical and biomedical ones [104–162].

## 6. Funding

The research was conducted as part of the scientific research task of the Ministry of Science and Higher Education of the Russian Federation (subject FZUN-2020-0013, state task of VIGU). The studies were carried out using the equipment of the interregional multidisciplinary and interdisciplinary center for the collective use of promising and competitive technologies in the areas of development and application in industry / mechanical engineering of domestic achievements in the field of nanotechnology (agreement No. 075-15-2021-692 dated August 5, 2021).

The research was partially supported by the Subsidy Agreement No. 075-15-2019-1838 dated December 6, 2019, FTP “Research and development in priority areas for the development of the scientific and technological complex for 2014-2020”, Activity 1.2, stage 1. Code: 2019-05-576-0001 “Development

of a multifunctional high-tech complex for layer-by-layer micro and nanomodification of surfaces of critical machine building parts using laser-hybrid technologies”.

## 7. Acknowledgments

The authors express their gratitude to Professor A.V. Kavokin, Associate Professor S.V. Kutrovskaya, Senior Researcher A.V. Osipov, Researcher T.A. Khudaiberganov for fruitful discussions, as well as Professor A.G. Tkachev for advice on carbon materials.

## 8. Conflict of interest

The authors declare no conflict of interest.

## References

1. Arakelyan SM, Kucherik AO, Prokoshev VG, Rau VG, Sergeev AG. *Introduction to Femtonanophotonics, Fundamentals and Laser Methods*. Tutorial. Moscow: Logos; 2015. 744 p. (In Russ.).
2. Gantmakher VF. *Electrons in disordered media*. 3rd ed. Moscow: Fizmatlit; 2013. 288 p. (In Russ.).
3. Ed. by Guowei Yang. *Laser ablation in liquids*. New York: Pan Stanford Publ.; 2012. 1192 p. DOI:10.1201/b11623
4. Kucherik AO, Arakelyan SM, Garnov SV, Kutrovskaya SV, Nogtev DS, Osipov AV, Khorkov KS. Two-stage laser-induced synthesis of linear carbon chains. *Kvantovaya elektronika = Quantum Electronics*. 2016;46(7):627-633. (In Russ.).
5. Kutrovskaya SV, Arakelian SM, Kucherik AO, Osipov AV, Garnov SV. Long linear carbon chain–laser-induced structures and possible applications. *Laser Physics*. 2019;29(8):085901. DOI:10.1088/1555-6611/ab183a
6. Cannella C, Goldman N. Carbyne fiber synthesis within evaporating metallic liquid carbon. *Journal of Physical Chemistry C*. 2015;119:21605-21611. DOI:10.1021/acs.jpcc.5b03781
7. Arakelian S, Kutrovskaya S, Kucherik A, Emel'yanov V, Zimin S. Laser-induced synthesis of nanostructured metal–carbon clusters and complexes. *Optical and Quantum Electronics*. 2016;48:3421-3416. DOI:10.1007/s11082-016-0776-7
8. Kucherik AO, Osipov AV, Arakelian SM, Garnov SV, Povolutckaya AV, Kutrovskaya SV. The laser-assisted synthesis of linear carbon chains stabilized by noble metal particle. *Journal of Physics: Conference Series*. 2019;1164:012006(1-7). DOI:10.1088/1742-6596/1164/1/012006
9. Amsler M, Flores-Livas J, Marques M. Prediction of a novel monoclinic carbon allotrope. *The European Physical Journal B*. 2013;86(9):1-3. DOI:10.1140/epjb/e2013-40639-4
10. Khorkov K, Kochuev D, Chkalov R, Prokoshev V, Arakelian S. Nonlinear dynamic processes in laser-induced

transitions to low-dimensional carbon nanostructures in bulk graphite unit. *Proceedings of the First International Nonlinear Dynamics Conference (NODYCON 2019), Springer Nature Switzerland*. 2020;3(131-140). DOI:10.1007/978-3-030-34724-6\_14

11. Bagayev SN, Arakelyan SM, Kucherik AO, Bukharov DN, Butkovskiy OYa. Nanooptics of thin-film laser-induced topological structures on a solid surface: fundamental phenomena and their applications. *Bulletin of the Russian Academy of Sciences: Physics*. 2020;84(12):1682-1695. DOI:10.3103/S1062873820120060 (In Russ.)

12. Kresin VV, Ovchinnikov YuN. Fast electronic relaxation in metal nanoclusters via excitation of coherent shape deformations. *Physical Review B – Condensed Matter and Materials Physics*. 2006;73:115412. DOI:10.1103/PhysRevB.73.115412

13. Abrikosov AA. *Fundamentals of the theory of metals*. Moscow: Nauka; 1987. 520 p. (In Russ.)

14. Sadakov AV, Sobolevsky OA, Pudalov VM. What led to the removal of the article on room temperature superconductivity from the journal Nature: a series of errors or falsification? *Uspekhi fizicheskikh nauk = Physics-Uspekhi*. 2022;192:12(1409-1412). DOI:10.3367/UFNe.2022.11.039265 (In Russ.)

15. Arakelian SM, Kucherik AO, Khudaberganov TA, Bukharov DN, Istratov AV, Khorkov KS, Osipov AV, Butkovskiy OY. Nanophysics in laser-induced cluster systems: topological quantum states in electrical conductivity and features of optical spectra – theory and experiment for dimensional effects. *Optical and Quantum Electronics*. 2020;52(3):202. DOI:10.1007/s11082-020-02308-6

16. Dong X, Oganov A, Cui H, Zhou X-F, Wang H-T. Electronegativity and chemical hardness of elements under pressure. *Proceedings of the National Academy of Sciences of the United States of America*. 2022;119(10):e2117416119. DOI:10.1073/pnas.2117416119

17. Frydman A. Erratum to: The superconductor insulator transition in systems of ultrasmall grains. *Physica C: Superconductivity and its Applications*. 2003;391(4):189-195. DOI:10.1016/S0921-4534(03)01356-X

18. Landau LD, Lifshitz EM. *Theoretical physics. Statistical physics. Part I*. Moscow: Fizmatlit; 2013. 620 p. (In Russ.)

19. Landau LD, Lifshitz EM. *Theoretical physics. Electrodynamics of continuous media*. Moscow: Fizmatlit; 2005. 656 p. (In Russ.)

20. Antipov AA, Arakelyan SM, Garnov SV, Kutrovskaya SV, Kucherik AO, Nogtev DS, Osipov AV. Laser ablation of carbon targets placed in a liquid. *Quantum Electronics*. 2015;45(8):731-735. DOI:10.1070/QE2015v045n08ABEH015681

21. Kutrovskaya SV, Antipov AA, Arakelyan SM, Kucherik AO, Osipov AV. Measurement of the electrophysical properties of metal microcontacts using fractal geometry methods for the analysis of atomic force microscopy data. *Poverkhnost'. Rentgenovskiy, sinkhrotronnyy i neytronnyy issledovaniya = Journal of Surface Investigation: X-Ray, Synchrotron and Neutron Techniques*. 2017;3(1):59-65. (In Russ.)

22. Jagdish N, Bhaumik A. Novel phase of carbon, ferromagnetism, and conversion into diamond. *Journal of Applied Physics*. 2015;118:215303. DOI:10.1063/1.4936595

23. Magomedov MN. On baric crystal fragmentation. *Physics of Solid State*. 2003;45(5):953-956. DOI:10.1134/1.1575343

24. Suvakov M, Tadic B. Modeling collective charge transport in nanoparticle assemblies. *Journal of Physics Condensed Matter*. 2010;22(16):163201. DOI:10.1088/0953-8984/22/16/163201

25. Parthasarathy R, Lin X, Elteto K, Rosenbaum TF, Jaeger HM. percolating through networks of random thresholds: finite temperature electron tunneling in metal nanocrystal arrays. *Physical Review Letters*. 2004;92(7):076801. DOI:10.1103/PhysRevLett.92.076801

26. Bukharov DN, Osipov AV, Arakelyan SM, Kucherik AO. Graph-analytical model of the electrical conductivity of a semiconductor island plumbum telluride nanofilm. *Journal of Physics: Conference Series*. 2019;1331(1):012008(1-8). DOI:10.1088/1742-6596/1331/1/012008

27. Antipov AA, Arakelian SM, Kutrovskaya S, Kucherik A, Nogtev D, Osipov A, Emelyanov V, Zimin S. Electrical conductivity of PbTe nanocluster structures with controlled topology: manifestation of macroscopic quantum effects. *Bulletin of the Russian Academy of Sciences: Physics*. 2016;80(7):896-906. DOI:10.3103/S1062873816070042

28. Butko VYu, DiTusa JF, Adams PW. Coulomb gap: how a metal film becomes an insulator. *Physical Review Letters*. 2000;84(7):1543-6. DOI:10.1103/PhysRevLett.84.1543

29. Bukharov DN, Kucherik AO, Arakelian SM. Modeling of electrical conductivity of labyrinth bimetallic nanofilms. *Journal of Physics: Conference Series*. 2019;1331:1:012017(1-7). DOI:10.1088/1742-6596/1331/1/012017

30. Arakelyan SM, Kucherik AO, Khudaberganov TA, Bukharov DN. Simulation of macroscopic quantum states in the functional properties of CVC laser-induced 4D topological nanoclusters in thin films on a solid surface. *Izvestiya RAN. Seriya Fizicheskaya*. 2020;84:322-327. DOI:10.31857/S0367676520030059 (In Russ.)

31. Moskalev PV. Analysis of the structure of a percolation cluster. *Zhurnal tekhnicheskoy fiziki = Technical Physics*. 2009;54(6):763-769. DOI:10.1134/S1063784209060012 (In Russ.)

32. Kruglyak YuA. Nanotransistor physics: 2D MOS electrostatics and virtual source model. *Nanosistemy, Nanomaterialy, Nanotekhnologii*. 2018;16(4):599-631. (In Russ.)

33. Kozadaev AS, Dubovitsky EV. Implementation of the wave algorithm for determining the shortest route on a plane when modeling paths with obstacles. *Vestnik TGU*. 2010;15(6):1926-1931. (In Russ.)

34. Zyabirov EV, Tokarev SP, Fedoseeva LI. Methods for determining the shortest path between graph vertices. *Uspekhi sovremennogo yestestvoznaniya*. 2011;7:113-114. (In Russ.)



35. Zimin SP, Gorlachev ES. *Nanostructured lead chalcogenides: monograph*. Yaroslavl: YarGU; 2011. 211 p. (In Russ.)
36. Bukharov DN, Lelekova AF, Kucherik AO, Antipov AA, Kutrovskaya SV. *Model of hopping electrical conductivity*. Certificates for registration of computer programs No. 2019663686. 22 October 2019. (In Russ.)
37. Kurdak C, Kim J, Farina LA, Lewis KM, Bai X, Rowe MP, Matzger AJ. Au nanoparticle clusters: a new system to model hopping conduction. *Turkish Journal of Physics*. 2003;27(5):419-426.
38. Bukharov DN, Kucherik AO, Arakelyan SM. Combined model of electrically conductive properties of a PbTe island nanofilm. Mathematical and computer modeling [Electronic resource]: *Proceedings of the 8th International scientific conference dedicated to the memory of A.L. Iosefera (Omsk, November 20, 2020)*. Omsk: OmGU Publ. House; p. 110-112 (In Russ.)
39. Pochtenny AE. *DC hopping conduction in intrinsic and extrinsic organic semiconductors: monograph*. Minsk: BGTU; 2016. 171 p. (In Russ.)
40. Samyshkin V, Lelekova A, Osipov A, Bukharov D, Skryabin I, Arakelian S, Kucherik A, Kutrovskaya S. Photosensitive free-standing ultra-thin carbyne-gold films. *Optical and Quantum Electronics*. 2019;51:394. DOI:10.1007/s11082-019-2114-3
41. Alves HWL, Neto ARR, Scolfaro LMR, Myers TH, Borges PD. Lattice contribution to the high dielectric constant of PbTe. *Physical Review B – Condensed Matter and Materials Physics*. 2013;87:115-120. DOI:10.1103/PhysRevB.87.115204
42. Bel'skii MD, Bocharov GS, Elets'kii AV, Sommerer TJ. Electric field enhancement in field-emission cathodes based on carbon nanotubes. *Technical Physics*. 2010;55(2):289-295. DOI:10.1134/S1063784210020210
43. Arakelian S, Emel'yanov V, Kutrovskaya S, Kucherik A, Zimin S. Laser-induced semiconductor nanocluster structures on the solid surface: new physical principles to construct the hybrid elements for photonics. *Optical and Quantum Electronics*. 2016;48(6):342. DOI:10.1007/s11082-016-0608-9
44. Venermo J, Sihvola A. Dielectric polarizability of circular cylinder. *Journal of Electrostatics*. 2005;63(2):101-107. DOI:10.1016/j.elstat.2004.09.001
45. Radkov AV, Malakhanov AA. *Methods for measuring the resistivity of semiconductor materials. Topical issues of technical sciences*. St. Petersburg: OOO Molodoy uchenyy Publ. House; 2019. p. 18-24. (In Russ.)
46. Afonsky AA, Dyakonov VP. *Electronic measurements in nanotechnologies and microelectronics*. Moscow: DMK Press; 2011. 688 p. (In Russ.)
47. Vasiliev IV. Features of measurement of specific and surface resistance by four-probe method. *Vektor vysokikh tekhnologiy*. 2020;2(47):8-14. (In Russ.)
48. Arakelyan SM, Bukharov DN, Istratov AV, Kutrovskaya SV, Kucherik AO, Osipov AV. Mathematical modeling and study of the electrical conductivity of island metal and semiconductor films. *Dinamika slozhnykh sistem XXI vek*. 2014;5:36-40. (In Russ.)
49. Bukharov DN, Osipov AV, Arakelian SM, Kucherik AO. Graph-analytical model of the electrical conductivity of a semiconductor island plumbum telluride nanofilm. *Journal of Physics: Conference Series*. 2019;1331:012008. DOI:10.1088/1742-6596/1331/1/012008
50. Bukharov DN, Arakelyan SM, Istratov AV, Samyshkin VD. PbTe island film hopping electrical conductivity model. *Journal of Physics: Conference Series*. 2019;1189:012017. DOI:10.1088/1742-6596/1189/1/012017
51. Belko AV, Nikitin AV, Skaskevich AA, Bachurina AYU, Sarosek SI. Models of fractal structures in composite systems based on polymers. *Vestnik Grodnenskogo gosudarstvennogo universiteta imeni Yanki Kupaly. Seriya 2. Matematika. Fizika. Informatika, vychislitel'naya tekhnika i upravleniye*. 2012;2:95-104. (In Russ.)
52. Antipov AA, Arakelyan SM, Kutrovskaya SV, Kucherik AO, Nogtev DS, Osipov AV, Emelyanov VI, Zimin SP. Electrical conductivity of PbTe nanocluster structures with controlled topology: manifestation of macroscopic quantum effects. *Izvestiya RAN. Seriya Fizicheskaya = Bulletin of the Russian Academy of Sciences: Physics*. 2016;80(7):818-827. (In Russ.)
53. Kavokin A, Kutrovskaya S, Kucherik A, Osipov A, Vartanyan T, Arakelian S. The crossover between tunnel and hopping conductivity in granulated films of noble metals. *Superlattices and Microstructures*. 2017;111:335-339. DOI:10.1016/j.spmi.2017.06.050
54. Chuprov SS, Meleshevich KA, Bogolepov VA, Adeev VM, Shchur DV, Rudyk ND. Deposition of a layer of carbon nanotubes on the surface of reactor alloys. *Nanosistemy, Nanomaterialy, Nanotekhnologii*. 2012;10(4):753-761.
55. Mahanta A, Sarmah H, Paul R, Choudhury G. Julia set and some of its properties. *International Journal of Applied Mathematics & Statistical Sciences (IJAMSS)*. 2016;5(2):99-124.
56. Iudin DI, Koposov EV. *Fractals: from simple to complex*. Nizhny Novgorod: NNGASU; 2012. 200 p. (In Russ.)
57. Kutrovskaya S, Samyshkin V, Lelekova A, Povolotskiy A, Osipov A, Arakelian S, Kavokin A, Kucherik A. Field-induced assembly of sp-sp<sup>2</sup> carbon sponges. *Nanomaterials*. 2021;11(3):763. DOI:10.3390/nano11030763
58. Osipov A, Kucherik A, Kutrovskaya S, Istratov A, Samyshkin V, Skryabin I, Novodvorskiy O, Arakelian S. The modeling of the light sensitive titanium dioxide microrolls doped by noble metal nanoparticles. *Journal of Physics: Conference Series*. 2019;1331(1):012024(1-5). DOI:10.1088/1742-6596/1331/1/012024
59. Berghoff D, Bühler J, Bonn M. Low-field onset of Wannier-Stark localization in a polycrystalline hybrid organic inorganic perovskite. *Nature Communications*. 2021;12:5719. DOI:10.1038/s41467-021-26021-4
60. Khudaiberganov T, Arakelian S, Kutrovskaya S, Kucherik A, Chestnov I. Spatial confinement of the optical



- Tamm states under patterned metal films. *Journal of Physics: Conference Series*. 2019;1164:012008(1-5). DOI:10.1088/1742-6596/1164/1/012008
61. Khudaiberganov T, Chestnov I, Arakelian S. Quantum statistics of light emitted from a pillar microcavity. *Applied Physics B*. 2022;128:117. DOI:10.1007/s00340-022-07835-6
62. Onari S, Kontani H. Nematic. Order in twisted bilayer graphene by valley + spin fluctuation interference mechanism. strongly correlated electrons. *Physical Review Letters*. 2022;128:066401. DOI:10.1103/PhysRevLett.128.066401
63. Onari S, Kontani H. SU(4)valley+spin fluctuation interference mechanism for nematic order in magic-angle twisted bilayer graphene: the impact of vertex corrections. *Physical Review Letters*. 2022;11.128(6):066401. DOI:10.1103/PhysRevLett.128.066401
64. Pan B, Xiao J, Li J, Liu P, Wang C, Yang G. Carbyne with finite length: The one-dimensional sp carbon. *Science Advances*. 2015;1(9):e1500857-e1500857. DOI:10.1126/sciadv.1500857
65. Arakelian S, Chestnov I, Istratov A, Khudaiberganov T, Butkovskiy O. Nonlinear dynamic modeling for high temperature superconductivity in nanocluster topological structures on solid surface (New Trends in Nonlinear Dynamics. *Proceedings of the First International Nonlinear Dynamics. Proceedings of the First International Nonlinear Dynamics Conference (NODYCON 2019) Springer, Cham* 3. 2020;121-130.
66. Samyshkin V, Lelekova A, Osipov A, Bukharov D, Skryabin I, Arakelian S, Kucherik A, Kutrovskaya S. Photosensitive free standing ultra thin carbide-gold films. *Optical and Quantum Electronics*. 2019;51(12):394(1-9). DOI:10.48550/arXiv.1910.11008
67. Memetova A, Tyagi I, Karri RR, Singh P, Goscianska J, Memetov N, Zelenin A, Gerasimova A, Tkachev A, Babkin A, Shuklinov A, Dehghani MH, Agarwal S. Synthesis of carbon energized materials with directed regulation of specific surface and pore structure as potential adsorbent for methane mitigation. *Journal of Environmental Chemical Engineering*. 2022;10(6):108929. DOI: 10.1016/j.jece.2022.108929
68. Vasilets V, Shulga Y, Kabachkov E, Melezhik A, Tkachev A. Photooxidative resistance of polytetrafluoroethylene-graphene nanocomposites to vacuum ultraviolet radiation. *High Energy Chemistry*. 2021;55:280-284. DOI:10.1134/S0018143921040147
69. Fomkin AA, Pribylov AA, Shkolin AV, Men'shchikov IE, Pulin AL, Zhedulov SA, Tkachev AG, Memetov NR, Melezhik AV, Kucherova AE, Shubin IN. Methane adsorption in microporous carbon adsorbent with a bimodal pore size distribution. *Protection of Metals and Physical Chemistry of Surfaces*. 2020;56:1-5. DOI:10.1134/S2070205120010074
70. Goncharova IS, Polunin IA, Polunin KE, Buryak AK. Synthesis and sorption properties of metal-carbon sorbent based on shungite modified with silver. *Sorbtsionnye i khromatograficheskie protsessy*. 2018; 18(5):659-667. DOI:10.17308/sorpchrom.2018.18/592. (In Russ.)
71. Ali I, Basheer A A, Kucherova A, Memetov N, Pasko T, Ovchinnikov K, Pershin V, Kuznetsov D, Galunin E, Grachev V, Tkachev A. Advances in carbon nanomaterials as lubricants modifiers. *Journal of Molecular Liquids*. 2019;279:251-266. DOI:10.1016/j.molliq.2019.01.113
72. Burakova IV, Troshkina ID, Burakov AE, Zhukova OA, Wei MA, Neskornomnaya EA, Tkachev AG. Nanomodified activated carbons for removal of scandium and cerium ions from sulphate solutions. *Perspektivnye Materialy = Inorganic Materials: Applied Research*. 2019;9:44-53. DOI:10.30791/1028-978x-2019-9-44-53
73. Burakova IV, Burakov AE, Tkachev AG, Troshkina ID, Veselova OA, Babkin AV, Wei MA, Ali I. Kinetics of the adsorption of scandium and cerium ions in sulfuric acid solutions on a nanomodified activated carbon. *Journal of Molecular Liquids*. 2018;253:277-283. DOI:10.1016/j.molliq.2018.01.063
74. Jianjun Y, Shiqiu L, Qing L, Xikai W, Zhigang G, Yuqing Z, Xiaomeng W, Jian S, Xianhui C. Record-high-Tc elemental superconductivity in scandium. *Physical Review Letters*. 2023;130:256002. DOI:10.1103/PhysRevLett.130.256002
75. Ferini G, Baratta G, Palumbo ME. A Raman study of ion irradiated icy mixtures. *Astronomy & Astrophysics*. 2004;414:757-766. DOI:10.1051/0004-6361:20031641
76. Lozovik YE, Popov AM. Formation and growth of carbon nanostructures – fullerenes, nanoparticles, nanotubes and cones. *Physics-Uspekhi*. 1997;40(7):717-737. DOI:10.1070/PU1997v040n07ABEH000253
77. Faoro L, Feigel'man MV, Ioffe L. Non-ergodic extended phase of the Quantum Random Energy model. *Annals of Physics*. 2019;409(8):167916. DOI:10.1016/j.aop.2019.167916
78. Punnoose A, Finkel'stein AM. Metal-insulator transition in disordered two-dimensional electron systems. *Science*. 2005;310(5746):289-291. DOI:10.1126/science.1115660
79. Yugay KN. Topological superconductivity of nanostructures. *Vestnik OmGU*. 2013;2(68):104-107. (In Russ.)
80. Wu H, Wang Y, Xu Y, Sivakumar P, Pasco C, Filippozzi U, Parkin S, Zeng Y, McQueen T, Ali M. The field-free Josephson diode in a van der Waals heterostructure. *Nature*. 2022;604:653-656. DOI:10.1038/s41586-022-04504-8
81. Kang M, Fang S, Kim J, Ortiz B, Ryu S, Kim J, Yoo J, Sangiovanni G, Di Sante D, Park B, Jozwiak C, Bostwick A, Rotenberg E, Kaxiras E, Wilson S, Park J, Comin R. Twofold van hove singularity and origin of charge order in topological kagome superconductor CsV3Sb5. *Nature Physics*. 2022;18:301-308. DOI:10.1038/s41567-021-01451-5
82. Arakelian S, Bukharov D, Emel'yanov V, Zimin S, Kutrovskaya S, Kucherik A, Makarov A, Osipov A. Laser nanostructuring of the PbX thin films for creation of the semiconductor devices with controlled properties. *Physics*

*Procedia*. 2014;56:1115-1125. DOI:10.1016/j.phpro.2014.08.026

83. Römer GRBE, Huisin't Veld AJ. Matlab laser toolbox. *Physics Procedia*. 2010;5:413-419. DOI:10.1016/j.phpro.2010.08.068

84. Kashtanov PV. Nanoclusters: properties and processes. *Teplofizika Vysokikh Temperatur = High Temperature*. 2010;48(6):886-900. (In Russ.)

85. Eliseev AA, Lukashin AV. *Functional nanomaterials*. Moscow: Fizmatlit; 2010. 456 p. (In Russ.)

86. Rempel AA. Nanotechnologies. Properties and applications of nanostructured materials. *Russian Chemical Reviews*. 2007;76(5):435-461. DOI:10.1070/RC2007v076n05ABEH003674

87. Phan HT, Haes AJ. What Does Nanoparticle Stability Mean? *The Journal of Physical Chemistry C*. 2019;123(27):16495-16507. DOI:10.1021/acs.jpcc.9b00913

88. Roduner E. *Dimensional effects in nanomaterials*. Moscow: Technosphere; 2010. 368 p. (In Russ.)

89. Suzdalev IP, Buravtsev VN, Maksimov YuV, Imshennik VK, Novichikhin SV, Matveev VV, Plachind AS. Size effects and intercluster interactions in nanosystems. *Poluprovodnikovaya Svetotekhnika = Russian Journal of General Chemistry*. 2001;XLV(3):66-73. (In Russ.)

90. Dunyushkina LA. *Introduction to methods for obtaining film electrolytes for solid oxide fuel cells*. Monograph: Yekaterinburg; URO RAN. 2015. 126 p. (In Russ.)

91. Dubrovskiy VG, Tsyrlin GE. Growth kinetics of thin films under the germ mechanism of layer formation. *Fizika i tekhnika poluprovodnikov = Semiconductors*. 2005; 39(11):1312-1319. (In Russ.)

92. Hassa G. *Physics of Thin Films: Volume 3*. Moscow: Book on Demand; 2012. 331 p. (In Russ.)

93. Sidorova SV, Yurchenko PI. Investigation of the formation of island nanostructures in vacuum. *Nano- i Mikrosistemnaya Tekhnika*. 2011;5:9-11. (In Russ.)

94. Freik DM, Yurchyshyn IK, Lysyuk YuV. Quantum size effects in nanostructures and problems of thermoelectricity. *Termoelektrichestvo = Journal of Thermoelectricity*. 2012;2:5-30. (In Russ.)

95. Fedorov AV. *Optics of nanostructures*. St. Petersburg: Nedra; 2005. 181 p. (In Russ.)

96. Kulbachinsky VA. Semiconductor quantum dots. *Sorosovskiy obrazovatel'nyy zhurnal*. 2001;4:98-104. (In Russ.)

97. Laucht A, Hofbauer F, Hauke N, Angele J, Stobbe S, Kaniber M, Böhm G, Lodahl P, Amann M-C, Finley J. Electrical control of spontaneous emission and strong coupling for a single quantum dot. *New Journal of Physics*. 2009;11:023034. DOI:10.1088/1367-2630/11/2/023034

98. Sarkar DK, Zhou XJ, Tannous A, Louie M, Leung KT. Growth of self-assembled copper nanostructure on conducting polymer by electrodeposition. *Solid State Communications*. 2003;125:365-368. DOI:10.1016/S0038-1098(02)00883-9

99. Gribachev VV. Nanosensors. *Komponenty i tekhnologii*. 2009;4:21-24. (In Russ.)

100. Agrawal AA, Batageri GW, Blackburn WH, Bhattacharya SS. *Nanostructures in biomedicine*. Moscow: BINOM. Knowledge Lab; 2012. 519 p. (In Russ.)

101. Kryzhanovskaya NV, Maksimov MV, Zhukov AE. Lasers based on quantum dots and microcavities with whispering gallery modes. *Kvantovaya elektronika = Quantum Electronics*. 2014;44(3):189-200. (In Russ.)

102. Karachinsky L, Novikov I, Babichev A, Gladyshev A, Kolodeznyi E, Rochas S, Kurochkin A, Bobretsova Y, Klimov A, Denisov D, Voropaev K, Ionov A, Bougrov V, Egorov A. Optical gain in laser heterostructures with an active area based on an InGaAs/InGaAlAs superlattice. *Optics and Spectroscopy*. 2019;127:1053-1056. DOI:10.1134/S0030400X19120099

103. Slipchenko SO, Vinokurov DA, Pikhtin NA, Sokolova ZN, Stankevich AL, Tarasov IS, Alferov JL. Ultra-low internal optical losses in separate-confinement quantum-well laser heterostructures. *Fizika i tekhnika poluprovodnikov = Semiconductors*. 2004;38(12):1477-1486. (In Russ.)

104. Aseev AL. Nanomaterials and nanotechnologies for modern semiconductor electronics. *Rossiyskiye nanotekhnologii = Nanobiotechnology Reports*. 2006;1-2: 97-110. (In Russ.)

105. Krevchik VD. Quantum size effect and quantum tunneling with dissipation as the basis of ideas of modern nanoelectronics. Part I. Classical and quantum size effects. *Inzhiniring i tekhnologii*. 2016;1(1):1-18. (In Russ.)

106. Kruglyak YuA. Nanotransistor Physics: 2D MOS electrostatics and virtual source model. *Nanosistemy. Nanomaterialy, Nanotekhnologii*. 2018;16(4):599-631. (In Russ.)

107. Chuprov SS, Meleshevich KA, Bogolepov VA, Adeev VM, Shchur DV, Rudyk ND. Deposition of a layer of carbon nanotubes on the surface of reactor alloys. *Nanosistemy. Nanomaterialy, Nanotekhnologii*. 2012;10(4):753-761. (In Russ.)

108. Ilyichev EA, Nabiev RM, Petrukhin GN, Rychkov GS, Kuleshov AE, Migunov DM. Carbon materials in electronics: status and problems. *Izvestiya vysshikh uchebnykh zavedeniy. Elektronika = Russian Microelectronics*. 2011;5(91):18-35. (In Russ.)

109. Lysenko IE, Ezhova OA. Development and study of the design of a micromechanical linear acceleration sensor. *Izvestiya Yuzhnogo federal'nogo universiteta. Tekhnicheskiye nauki*. 2013:223-232. (In Russ.)

110. Achildiev VM, Gruzevich YuK, Soldatenkov VA. *Information measuring and optoelectronic systems based on micro- and nanomechanical sensors of angular velocity and linear acceleration*. Moscow: Bauman MGTU Publ. House; 2016. 260 p. (In Russ.)

111. Cao G. *Nanostructures and nanomaterials: Synthesis, Properties and Applications*. London: World Scientific Publishing; 2011. 581 p. (In Russ.)

112. Gulyakovich GN, Severtsev VN, Shurchkov IO. Prospects and problems of semiconductor nanoelectronics. *Inzhenernyy vestnik Dona*. 2012;2(20):315-319. (In Russ.)
113. John R, Vermesan O, Ottella M, Perlo P. Nanoelectronics: Key Enabler for Energy Efficient Electrical Vehicles. In: *Advanced Microsystems for Automotive Applications*. Berlin: Springer; 2009. p. 13-24. DOI:10.1007/978-3-642-00745-3\_2
114. Turkin AA. Semiconductor LEDs: history, facts, prospects. *Poluprovodnikovaya Svetotekhnika*. 2011;5:28-33. (In Russ.)
115. Dalvinder SG. Present and future nanoelectronics devices-an analytical study. *Research & Development in Material Science*. 2018;8(4):925-930. DOI:10.31031/RDMS.2018.08.000693
116. Alferov ZH, Aseev AL, Gaponov SV, Kopiev PS, Panov VI, Poltoratsky EA, Sibeldin NN, Suris RA. Nanomaterials and nanotechnologies. *Mikrosistemnaya tekhnika*. 2003;8:3-13. (In Russ.)
117. Moiseev SA, Andrianov SN, Moiseev ES. Quantum computer in the scheme of an atomic quantum transistor with logical coding of qubits. *Optika i spektroskopiya = Optics and Spectroscopy*. 2013;115(3):406-414. (In Russ.)
118. Loktev DD, Yamashkin EE. Methods and equipment for applying wear-resistant coatings. *Nanoindustriya*. 2007;4:18-24. (In Russ.)
119. Popescu C, Dorcioman G, Popescu A. Laser ablation applied for synthesis of thin films: insights into laser deposition methods. In: *Applications of laser ablation – thin film deposition, nanomaterial synthesis and surface modification*. IntechOpen; 2016. 426 p. DOI:10.5772/65124
120. Zuev DA, Lotin AA, Novodvorsky OA, Lebedev FV, Khranova OD, Petukhov IA, Putilin FN, Shatokhin AN, Rumyantseva MN, Gaskov AM. Pulsed laser deposition of ITO thin films and their characteristics. *Fizika i tekhnika poluprovodnikov = Semiconductors*. 2012;46(3):425-429. (In Russ.)
121. Eroshova OI, Perminov PA, Zabotnov SV, Gongalsky MB, Ezhov AA, Golovan LA, Kashkarov PK. Structural properties of silicon nanoparticles fabricated by pulsed laser ablation in liquid media. *Kristallografiya = Crystallography Reports*. 2012;57(6):942-947. (In Russ.)
122. Domke M, Nobile L, Rapp S, Eiselen S, Sotop J, Huber HP, Schmidt M. Understanding thin film laser ablation: the role of the effective penetration depth and the film thickness. *Physics Procedia*. 2014;56:1007-1014. DOI:10.1016/j.phpro.2014.08.012
123. Samarsky AA, Mikhailov AP. *Mathematical modeling: Ideas. Methods. Examples*. Moscow: Fizmatlit; 2005. 320 p. (In Russ.)
124. Smirnov VA, Korolev EV, Evstigneev AV. Modeling and numerical analysis tools in nanotechnology and materials science: a review. *Nano tekhnologii v stroitel'stve*. 2014; 6(5):34-58. (In Russ.)
125. Fedotov AY. Modeling of formation processes and properties of nanostructures and nanofilms formed in a gas medium. *Khimicheskaya fizika i mezoskopiya*. 2017;19(2):230-249. (In Russ.)
126. Wang J, Karihaloo B, Duan H, Huang Z. Importance of surface/interface effect to properties of materials at nano-scale. *Solid Mechanics and Its Applications*. 2006;135:227-234. DOI:10.1007/1-4020-4566-2\_26
127. Zinchenko LA, Shakhnov VA. Peculiarities of mathematical modeling in nanosystem design problems. *Nanotekhnologii. Informatsionnyye tekhnologii i vychislitel'nyye sistemy*. 2009;4:84-92. (In Russ.)
128. Rieth M, Schommers W. *Handbook of Theoretical and Computational Nanotechnology*. Philippe: American Scientific Publishers; 2006. 623 p.
129. Kabaldin YG. Information model of assembly of nanostructures. *Trudy Nizhegorodskogo gosudarstvennogo tekhnicheskogo universiteta im. R.E. Alekseyeva*. 2010;3(100):90-99. (In Russ.)
130. Tapilin VM. A new approach to the correlation gap: the value of the interelectrode interaction potential as a variable in solving the many-particle schrödinger equation. *Zhurnal strukturnoy khimii = Journal of Structural Chemistry*. 2008;49(3):407-414. (In Russ.)
131. Kholmurodov HT, Altai MV, Puzyrin IV, Dardin TA, Filatov FP. Molecular dynamics methods for modeling physical and biological processes. *Fizika elementarnykh chastits i atomnogo yadra = Physics of Particles and Nuclei*. 2003;34:2. (In Russ.)
132. Shilov MA, Veselov VV. *Computer modeling of molecular systems by the method of molecular dynamics*. Ivanovo: IGTA; 2010. 168 p. (In Russ.)
133. Grishko MS, Beznosyuk SA, Zhukovsky MS, Zhukovskaya TM. Monte Carlo computer simulation of the formation of nickel clusters in nanopores of materials. *Izvestiya Altayskogo gosudarstvennogo universiteta*. 2007;3:71-75. (In Russ.)
134. Kolesnikov SV, Saletsky AM, Dokukin SA, Klavsyuk AL. Kinetic Monte Carlo method: mathematical foundations and applications to the physics of low-dimensional nanostructures. *Matematicheskoye modelirovaniye = Mathematical Models and Computer Simulations*. 2018;30(2):48-80. (In Russ.)
135. Nastoviyak AG, Usenkova NL, Schwartz IG, Neizvestny IG. Features of the realization of the crystallization process in the Monte Carlo simulation of the growth of nanowiskers. *Izvestiya vuzov. Fizika = Russian Physics Journal*. 2009; 52(11):52-57. (In Russ.)
136. Suzdalev IP. *Nanotechnology: Physical chemistry of nanoclusters, nanostructures and nanomaterials*. Moscow: URSS; 2008. 589 p. (In Russ.)
137. Redel LV, Gafner YuYa, Gafner SL. The role of “magic” numbers in structure formation in small silver nanoclusters. *Fizika tverdogo tela = Physics of the Solid State*. 2015;57(10):2061-2070. (In Russ.)



138. Mazalova VL, Kravtsova AN, Soldatov AV. *Nanoclusters: X-ray spectral studies and computer simulation*. Moscow: FIZMATLIT; 2013. 184 p. (In Russ.)
139. Derevianko AI. Computer simulation of phase transition dynamics in aggregation processes. *Adaptivnyye sistemy avtomaticheskogo upravleniya: mezhdvdomstvennyy nauchno-tekhnicheskij sbornik*. 2005;8(28):11-15. (In Russ.)
140. Roldugin VI. Fractal structures in dispersed systems. *Uspekhi khimii = Russian Chemical Reviews*. 2003;72(10):931-959. (In Russ.)
141. Zyryanov RS. Development of fractal models of aggregation of colloidal particles. *Molodoy uchenyy*. 2016;24(128):72-76. (In Russ.)
142. Wei H. From silver nanoparticles to thin films: Evolution of microstructure and electrical conduction on glass substrates. *Journal of Physics and Chemistry of Solids*. 2009;70:459-465. DOI:10.1016/j.jpcs.2008.11.012
143. Gladskikh IA, Polishchuk VA, Vartanyan TA. Silver structures at the percolation threshold, prepared by laser annealing. *Physics of the Solid State*. 2017;59:601-606. DOI:10.1134/S106378341703012X
144. Lysenkov EA, Klepko VV, Yakovlev YuV. Features of the percolation behavior of systems based on polyesters and carbon nanotubes with the addition of LiClO<sub>4</sub>. *Elektronnaya obrabotka materialov = Surface Engineering and Applied Electrochemistry*. 2016;52(2):62-68. (In Russ.)
145. Trachtenberg LI, Melnikov MYa. *Synthesis, structure and properties of metal/semiconductor containing nanostructured composites*. Moscow: Technosphere; 2016. 624 p. (In Russ.)
146. Rostovshchikova TN, Smirnov VV, Kozhevnikov VM, Yavsin DA, Gurevich SA. Intercluster interactions in catalysis by nanosized metal particles. *Rossiyskiye nanotekhnologii = Nanobiotechnology Reports*. 2007;2(1-2):47-60. (In Russ.)
147. Vartanyan TA, Gladskikh IA, Leonov NB, Przhibelsky SG. Fine structures and electrical conductivity switching in silver labyrinth films on sapphire. *Fizika tverdogo tela = Physics of the Solid State*. 2014;56(4):783-789. (In Russ.)
148. Fateev MP. Hopping transport theory in disordered systems. *Fizika tverdogo tela = Physics of the Solid State*. 2010;52(6):1053-1059. (In Russ.)
149. Bleibaum O, Böttger H, Bryksin VV. Random-resistor network description for hopping transport in the presence of Hubbard interaction. *Journal of Physics: Condensed Matter*. 2003;15:1719. DOI:10.1088/0953-8984/15/10/319
150. Faggionato A, Mimun HA. Connection probabilities in Poisson random graphs with uniformly bounded edges. *Alea*. 2019;16:463-486. DOI:10.30757/ALEA.v16-18
151. Wagner S, Pundt A. Conduction mechanisms during the growth of the Pd thin films: experiment and model. *Physical Review B – Condensed Matter and Materials Physics*. 2008;78:155131. DOI:10.1103/PhysRevB.78.155131
152. Sieradzki K, Bailey K, Alford TL. Agglomeration and percolation conductivity. *Applied Physics Letters*. 2001;79:3401-3403. DOI:10.1063/1.1419043
153. Kornushchenko AS, Natalich VV, Perekrestov VI, Kosminska YO. Obtaining, structure and sensory properties of fractal-percolation ZnO. *Journal of Nano- and Electronic Physics*. 2018;10:06021. DOI:10.21272/jnep.10(6).06021
154. Fedorovich R, Naumovets A, Tomchuk P. Electronic properties of island thin films caused by surface scattering of electrons. *Progress in Surface Science*. 2000;328:73-179. DOI:10.1016/0079-6816(93)90069-8
155. Saifutiyarov RR, Khomyakov AV, Mozhevitina EN, Avetisov IKh. Nanoscale films of cadmium and zinc selenides with controlled nonschometry. *Uspekhi v khimii i khimicheskoy tekhnologii*. 2014;6:28-30. (In Russ.)
156. Boltaev AP, Penin NA, Pogosov AO, Pudonin FA. Activation conductivity in island metal films. *Zhurnal Eksperimental'noy i Teoreticheskoy Fiziki = Journal of Experimental and Theoretical Physics*. 2004;126:954-961. (In Russ.)
157. Ravich Yu. Hopping conduction over strongly localized states of indium in PbTe and solid solutions based on it. *Fizika i tekhnika poluprovodnikov = Semiconductors*. 2002;36(1):3-23. (In Russ.)
158. Anfimov IM, Kobeleva SP, Malinkovich MD, Shemerov IV, Toropova OV, Parkhomenko YuN. Electrical conductivity mechanisms of silicon-carbon nanocomposites with nanosized tungsten inclusions in the temperature range 20–200 °C. *Materialy elektronnoy tekhniki*. 2012;2:58-60. (In Russ.)
159. Yu D, Wang C, Wehrenberg BL, Guyot-Sionnest P. Variable range hopping conduction in semiconductor nanocrystal solids. *Physical Review Letters*. 2004;92(21):216802. DOI:10.1103/PhysRevLett.92.216802
160. Gallyamov SR, Melchukov SA. Percolation model of two-phase lattice conductivity: theory and computer experiment. *Vestnik Udmurtskogo Universiteta. Matematika. Mekhanika. Komp'yuternyye nauki*. 2010;4:112-122. (In Russ.)
161. Aleskerov FK, Kakhramanov KSH, Kakhramanov SSH. Percolation effect in Bi<sub>2</sub>Te<sub>3</sub> crystals doped with copper or nickel. *Neorganicheskiye materialy = Inorganic Materials*. 2012;48(5):536-541. (In Russ.)
162. Melezhyk AV, Tkachev AG. Synthesis of graphene nanoplatelets from peroxosulfate graphite interaction compounds. *Nanosystems: Physics, Chemistry, Mathematics*. 2014;5(2):294-306.



### Information about the authors / Информация об авторах

**Dmitry N. Bukharov**, Senior Lecturer, Vladimir State University A.G. and N.G. Stoletovs, Vladimir, Russian Federation; ORCID 0000-0002-4536-8576; e-mail: bukharov@vlsu.ru

**Alexey O. Kucherik**, D. Sc. (Phys. and Math.), Associate Professor, Vice-Rector for Research and Digital Development, Vladimir State University A.G. and N.G. Stoletovs, Vladimir, Russian Federation; ORCID 0000-0003-0589-9265; e-mail: kucherik@vlsu.ru

**Sergei M. Arakelian**, D. Sc. (Phys. and Math.), Professor, Head of Department, Vladimir State University A.G. and N.G. Stoletovs, Vladimir, Russian Federation; ORCID 0000-0002-6323-7123; e-mail: arak@vlsu.ru

**Бухаров Дмитрий Николаевич**, старший преподаватель, Владимирский государственный университет им. А. Г. и Н. Г. Столетовых, Владимир, Российская Федерация; ORCID 0000-0002-4536-8576; e-mail: bukharov@vlsu.ru

**Кучерик Алексей Олегович**, доктор физико-математических наук, доцент, проректор по научной работе и цифровому развитию, Владимирский государственный университет им. А. Г. и Н. Г. Столетовых, Владимир, Российская Федерация; ORCID 0000-0003-0589-9265; e-mail: kucherik@vlsu.ru

**Аракелян Сергей Мартиросович**, доктор физико-математических наук, профессор, заведующий кафедрой, Владимирский государственный университет им. А. Г. и Н. Г. Столетовых, Владимир, Российская Федерация; ORCID 0000-0002-6323-7123; e-mail: arak@vlsu.ru

*Received 13 June 2023; Accepted 28 July 2023; Published 06 October 2023*



**Copyright:** © Bukharov DN, Kucherik AO, Arakelian SM, 2023. This article is an open access article distributed under the terms and conditions of the Creative Commons Attribution (CC BY) license (<https://creativecommons.org/licenses/by/4.0/>).